(4)

NUSC Technical Report 8537
June 1989

Wind Speed Dependence of Acoustic Ambient Vertical Directional Spectra at High Frequency

R.M. Kennedy
T.K. Szlyk
S.M. Wentworth
Test and Evaluation Department
West Palm Beach, Florida

Naval Underwater Systems Center
Newport, Rhode Island / New London, Connecticut

PREFACE

This report was prepared under project B64838 and 638V11, Principal Investigator R.M. Kennedy (Code 3802). The work reported herein was performed as part of the Naval Underwater Systems Center program of Independent Research and Independent Exploratory Development (IR/IED), Program Manager Dr. K.M. Lima, and the Test and Evaluation Department Acoustic Range Initiative, Program Manager J.H. Keegan.

The Technical Reviewer for this report was A.B. Caron (Code 38202) whose contributions to the report are gratefully acknowledged.

Reviewed and Approved: August 1989

J.H. Keegan, Code 38
Head, Test and Evaluation Department

UNCLASSIFIED
SECURITY CLASSIFICATION OF THIS PAGE

REPORT DOCUMENTATION PAGE

1a. REPORT SECURITY CLASSIFICATION **Unclassified**	1b. RESTRICTIVE MARKINGS
2a. SECURITY CLASSIFICATION AUTHORITY	3. DISTRIBUTION / AVAILABILITY OF REPORT **Approved for public release, distribution is unlimited.**
2b. DECLASSIFICATION / DOWNGRADING SCHEDULE	
4. PERFORMING ORGANIZATION REPORT NUMBER(S) **TR 8537**	5. MONITORING ORGANIZATION REPORT NUMBER(S)
6a. NAME OF PERFORMING ORGANIZATION **Naval Underwater Systems Center Detachment** 6b. OFFICE SYMBOL (*If applicable*) **3802**	7a. NAME OF MONITORING ORGANIZATION
6c. ADDRESS (*City, State, and ZIP Code*) **West Palm Beach, FL 33402**	7b. ADDRESS (*City, State, and ZIP Code*)
8a. NAME OF FUNDING / SPONSORING ORGANIZATION **Naval Underwater Systems Center** 8b. OFFICE SYMBOL (*If applicable*) **38**	9. PROCUREMENT INSTRUMENT IDENTIFICATION NUMBER
8c. ADDRESS (*City, State, and ZIP Code*) **Newport, RI 02841**	10. SOURCE OF FUNDING NUMBERS PROGRAM ELEMENT NO. / PROJECT NO. **638V11** / TASK NO. / WORK UNIT ACCESSION NO.

11. TITLE (*Include Security Classification*)
Wind Speed Dependence of Acoustic Ambient Vertical Directional Spectra at High Frequency

12. PERSONAL AUTHOR(S)
Kennedy, R.M. Szlyk, T.K. Wentworth, S.M.

13a. TYPE OF REPORT	13b. TIME COVERED	14. DATE OF REPORT (*Year, Month, Day*)	15. PAGE COUNT
Final	FROM _____ TO _____	**1989 June**	**60**

16. SUPPLEMENTARY NOTATION

17. COSATI CODES			18. SUBJECT TERMS (*Continue on reverse if necessary and identify by block number*)
FIELD	GROUP	SUB-GROUP	**Underwater Acoustics**
17	01		

19. ABSTRACT (*Continue on reverse if necessary and identify by block number*)

See reverse side.

20 DISTRIBUTION / AVAILABILITY OF ABSTRACT ☐ UNCLASSIFIED/UNLIMITED ☒ SAME AS RPT. ☐ DTIC USERS	21. ABSTRACT SECURITY CLASSIFICATION **Unclassified**
22a NAME OF RESPONSIBLE INDIVIDUAL **R.M. Kennedy**	22b. TELEPHONE (*Include Area Code*) **(407) 832-8566** 22c. OFFICE SYMBOL **3802**

DD FORM 1473, 84 MAR 83 APR edition may be used until exhausted.
All other editions are obsolete.

SECURITY CLASSIFICATION OF THIS PAGE
UNCLASSIFIED

19. ABSTRACT

A measurement of the acoustic ambient arriving from a horizontal direction along with total acoustic intensity spectra allows one to infer both the total directional spectra and some physical characteristics of the sources of "sea surface sound." A long-term measurement of these two quantities was made at high frequency, i.e., 8 kHz to 64 kHz, in the Tongue of the Ocean, The Bahamas. The horizontally directed ambient was measured using vertically oriented line arrays and was observed for wind speeds ranging from 1 to 30 knots. The resulting data base was used to estimate the statistics of anisotropic "noise gain" relative to the isotropic "noise gain." Differences in the functional dependence and residual statistics were found for two cases: whitecaps present and not present. The relation of these results to the total directional spectra and a model of the near-surface distribution of acoustic sources are discussed.

SUMMARY

This report describes the results of a data analysis task that estimated the acoustic ambient directional spectra caused by sea surface sources of sound from measurements of the horizontally directed acoustic ambient. A theoretical discussion shows that the near-horizontal value of the directional spectra is a sensitive measure of the entire directional spectra resulting from a diffuse source field consisting of surface dipoles and a subsurface layer of monopoles. An extended measurement was undertaken of the horizontal value of the array gain of three vertical arrays covering the frequency range of 8 to 32 kHz. Measurements of the array gain and the total acoustic intensity were made over a 1-year period along with a nearby measurement of the wind speed at a 10-m height. These measurements took place in The Tongue of the Ocean in The Bahamas, at a depth of 125 m in 1830 m of water. The results of the analysis indicated a clear wind speed dependence in the horizontally steered array gain resulting from a wind speed dependence in the acoustic ambient vertical directional spectra. The measured acoustic sound pressure level spectra were shown to agree well with previous measurements. The observed array gain was found to dichotomize into categories of either whitecaps present or whitecaps not present, with distinctly different behavior in each category. With whitecaps present the array gain was found to be greater than the directivity index of the array because the ambient pressure field was dominated by energy arriving nearly vertical to the array. This is characteristic of a source field of surface dipoles, presumably caused by whitecap generation of both spray and an acoustically thin layer of bubbles. Surface dipoles cause a maximum array gain condition which was observed in the data by examining the statistical distribution of array gain values. This distribution was found to be skewed to lower values of gain, indicating the existence of a physical maximum in array gain caused by dipole sources. When whitecaps were not present the array gain, relative to the directivity index, was lower than in the case with whitecaps present. While there was significant variability in the array gain for a given wind speed, the array gain in general followed a power law model with a 1.9 exponent. The reduction in array gain was

caused by an increase in the horizontal values of the vertical directional spectra relative to the vertical value. It is shown that this situation could be caused by an acoustically thick sublayer of monopoles, presumably bubbles. If this model is correct, the depth scale of the vertical distribution of the bubble density is inversely proportional to wind speed. However, it is clear from the variability of the array gain at a given wind speed that wind is only one of several causes of the change in the sublayer depth scale. The data show, at least for this high frequency range, the wind speed dependence of the acoustic ambient near-horizontal directional spectra inferred from the array gain measurements. It is shown that total acoustic sound pressure level spectra is a better predictor of array gain than is the wind speed. This last result indicates that when whitecaps are not present the wind speed is not a complete indication of the acoustic state of the sea and, furthermore, that total acoustic sound pressure level is related to the vertical directional spectra of the sea surface-caused sound.

TABLE OF CONTENTS

LIST OF ILLUSTRATIONS

LIST OF ILLUSTRATIONS (Cont'd)

1.0 INTRODUCTION

The experiment described in this technical report was based on measurements of opportunity. The experiment was not specifically designed to meet the objectives stated below. Rather, a data set became available which appears to offer additional insight into the space-time characterization of "sea surface sound" generated acoustic ambient. Such a statistical characterization of an important source of natural underwater acoustic noise has clear relevance to the design of systems intended to detect and measure underwater acoustic radiation. The analysis of the data set was undertaken to meet the objective of determining the wind speed dependence of high frequency vertical directional spectra caused by "sea surface sound."

Significant literature[1-4] has been devoted to this subject; however, there is no established physical theory of surface noise generation at frequencies above approximately 50 Hz.[5,6] "Bubbles and spray" theories applicable to the frequencies of interest exist[7-9] but have not been adequately tested or integrated into space-time statistical descriptions. Below the wind speed for which incipient whitecapping exists, there is even less known.[10] The historical approach to anisotropic ambient modeling is a "source plane" description[11] derived from hydrophone array measurements.[12] Thus the modeling efforts are data driven because of the lack of a basic source description, and the data base is flawed because much of the data was taken in open ocean areas where shipping[13] and sea conditions well removed from the measurement[14] dominated the vertical anisotropic field. In this experiment external contamination of the data is controlled by the location of the experiment, The Tongue of the Ocean (TOTO) in The Bahamas, and the high frequencies measured (8 to 64 kHz). The location is a relatively deep (1830 meters) body of water isolated from global shipping.

The next section of this report gives a theoretical view of the role of a near-surface layer of monopoles, in contrast with the more familiar surface distribution of dipoles, in determining the acoustic directional spectra. That section is followed by a description of the experiment and the data

analysis techniques. The final sections include a detailed analysis of the results and conclusions.

2.0 THEORY

In this section analytical expressions are developed for the vertical directional spectra caused by a diffuse layer of monopole sources beneath an arbitrarily rough "pressure release" surface. The density of the monopole sources is assumed to be uniformly distributed in the horizontal direction, and either exponential or uniform distributions are considered in the vertical direction. The objective is to predict the change in the horizontally directed acoustic field due to a change in the near-surface acoustic source distribution. The effort explores the hypothesis that the origin of the acoustic ambient changes from momentum fluctuations on the boundary when whitecaps are present to bubble oscillation beneath the surface in the absence of whitecaps.

We wish to model a monopole source at a depth z_0 beneath the surface as pictured in figure 1a; i.e., the positive z axis is below the surface. At a later point we will consider a monopole density function. However, here we express the pressure field of a single monopole source in the vicinity of the monopole, i.e., at a radial distance R, as

$$P = P_0/R \ , \tag{1}$$

where $P_0 = Q/4\pi$ and Q is the monopole source strength. The received pressure at a large distance from the monopole source is

$${}_0P_r = \left[\frac{e^{-nR}}{R}e^{ikR} - \gamma\frac{e^{-nR'}}{R'}e^{ikR'}\right]P_0e_0^{-iwt} \ , \tag{2}$$

where the real variable n is the water attenuation coefficient, γ is a complex-valued reflection loss coefficient, and k is the wavenumber magnitude in the radial direction of propagation. It is useful to write the surface reflection coefficient in polar form as

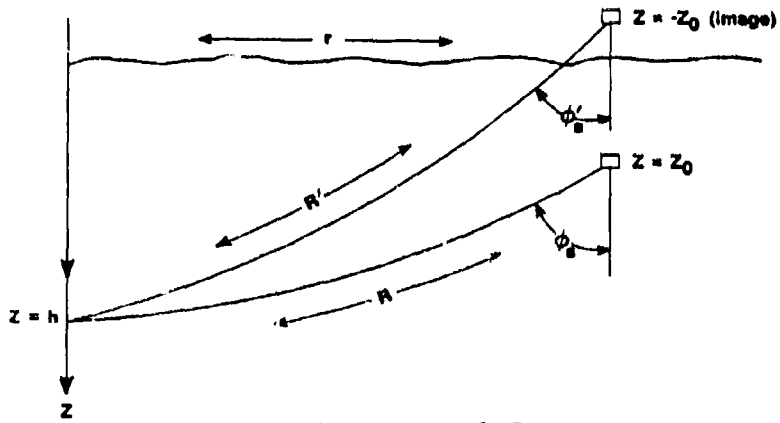

(a) General Case

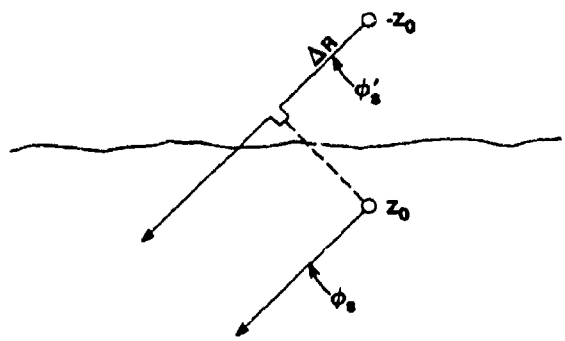

(b) Deep Receiver, Shallow Source Case

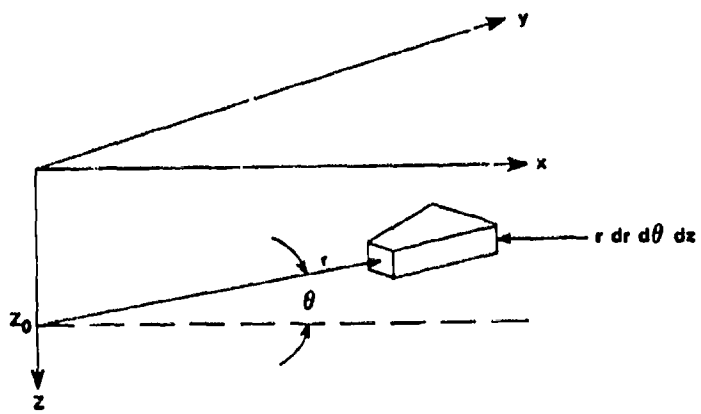

(c) Differential Source Volume

Figure 1. Spatial Relationships

$$\gamma = \mu e^{-i2k\zeta \cos\phi} , \tag{3}$$

where μ is an amplitude reflection coefficient[15] and $(2k\zeta \cos\phi)$ is a phase change[16] from a reflection from a "rough" surface of height ζ relative to the mean height of $\zeta = 0$.

The mean-square received pressure becomes

$$\overline{{}_0P_r^2} = (P_0)^2 \left[\left(\frac{e^{-nR}}{R} \right)^2 + \overline{|\gamma|}^2 \left(\frac{e^{-nR'}}{R'} \right)^2 - 2 \left(\frac{e^{-nR}}{R} \right) \left(\frac{e^{-nR'}}{R'} \right) R_e \left(\overline{\gamma} e^{ik\Delta R} \right) \right] , \tag{4}$$

where the bar denotes time average, and $\Delta R = R - R'$.

Note that equation (4) will be realized only if the receiver's spatial resolution is unable to separate the two paths. If the receiver is capable of resolving the two paths, then the strengths of the monopole and its image will be observed separately. The separability of the two arrivals is a function of the ratio of the source and receiver depths (z_0/h). For the case of interest, for which the receiver depth is much greater than the maximum source depth $(z_0/h \ll 1)$, the receiver observes the monopole and image arrival from the same angle but with a phase delay $(k\Delta R)$. Figure 1 shows that if $\phi_s \simeq \phi_s'$ then

$$R = \int_{z_0}^{h} \frac{dz}{\cos\phi(z)} , \text{ and} \tag{5a}$$

$$R' = R + \int_{-z_0}^{z_0} \frac{dz}{\cos\phi_s(z)} \simeq R + \frac{2z_0}{\cos\phi_s} , \tag{5b}$$

where we have neglected refraction effects only over the short spatial interval $-z_0$ to z_0. Thus while $R' \simeq R$ we have

$$\Delta R = 2z_0 \cos\phi_s \ . \tag{6}$$

In light of these approximations, equation (4) becomes

$$\overline{{}_0P_r^2} = \left(\frac{P_0}{R}\right)^2 e^{-2n\bar{R}}\left[1 + \overline{|\gamma|^2} - 2R_e\left(\bar{\gamma}e^{ik\Delta R}\right)\right] \ . \tag{7}$$

The amplitude reflection coefficient[15] is

$$\overline{|\gamma|^2} = \overline{\mu^2} = e^{-2k\sigma \cos\phi_s} \ , \tag{8}$$

where σ is the root-mean-square surface roughness. We assert that the random phase and amplitude components of the complex reflection coefficient, equation (4), are statistically independent, and

$$\bar{\gamma} = \overline{\mu e^{i2k\zeta \cos\phi}} \ ,$$

where

$$\overline{e^{ik\zeta \cos\phi}} = \int_{-\infty}^{\infty} d\zeta \ \frac{e^{-\frac{\zeta^2}{2\sigma^2}}}{\sigma\sqrt{2\pi}} \ e^{i2k\zeta \cos\phi_s} = e^{-2k^2\sigma^2 \cos\phi_s^2} \tag{9}$$

for a Gaussian distributed surface elevation.[16] Thus, by using equation (9), equation (7) becomes

$$\overline{{}_0P_r^2} = \left(\frac{P_0}{R}\right)^2 e^{-2nR}\left[\left(1 + e^{-2k^2\sigma^2 \cos^2\phi_s}\right)\right. \tag{10}$$

$$\left. -2e^{-k^2\sigma^2 \cos^2\phi_s} \cos\left(2kz_0 \cos\phi_s\right)\right] .$$

For a perfectly smooth surface this becomes the familiar "dipole"

$$\overline{P_r^2} = 4\left(\frac{P_0}{R}\right)^2 e^{-2nR} \sin^2\left[kz_0 \cos\phi_s\right] . \tag{11}$$

If there are $N_M(z)$ statistically independent monopoles per unit volume, then

$$P^2 = N_M(z)P_0^2 \tag{12}$$

is the monopole source pressure level per unit volume and $d\overline{P_r^2}(z)$ is the received mean-square pressure level per unit source volume at range R from the receiver.

The differential received mean-square pressure level due to a differential source volume (r dr dθ dz) located at r, θ, and z is

$$d\overline{p_r^2}(z) = \overline{p_r^2}\ r\ dr\ d\theta\ dz \tag{13}$$

and the receiver directional spectral function is

$$N_M(\phi,\theta) = \frac{\overline{p_r^2}\ r\ dr\ d\theta}{d\psi}\ dz = \overline{p_r^2}\ \frac{dA}{d\psi}\ dz , \tag{14}$$

where $d\psi$ is the differential solid angle measured at the receiver, and the differential volume (dA dz) is measured at the source. This problem historically has been solved[15] for a source "plane" which involves only the differential area. Each differential source area contributes to a unique receiver elevation angle. For the "volume" source case there is no longer a unique relation between each differential source volume and a receiver elevation angle. This point is most easily illustrated for the isovelocity case for which $\phi = \phi_s$ and

$$\tan\phi = \frac{r}{h - z_0} \quad \text{for } \pi/2 \le \phi \le \pi \ .$$

Thus for a "source plane" both h and z_0 are constant and r uniquely determines ϕ. In general there is a differential "tube" of sources which contribute to a specific elevation angle. The total acoustic intensity associated with a specific direction, θ and ϕ, is determined by integrating along the tube, i.e., incoherently summing all of independent acoustic sources contributing to a specific direction. Within the limits of our deep receiver-shallow source assumption, i.e., D/h << 1, all of the sources in the volume

$$\int_0^D dz\ r\ dr\ d\theta$$

contribute to a unique direction. Thus we may express the desired directional spectra as

$$N_M(\theta,\phi) = \int_0^D dz\ \frac{\overline{dp_r^2(z)}}{d\psi} = \int_0^D dz\ \frac{\overline{p_r^2(z)}\ d\theta\ r\ dr}{d\phi\ d\theta\ \sin\phi} \ , \text{ and} \tag{15a}$$

$$N_M(\theta,\phi) = \int_0^D \frac{\overline{p_r^2(r,\ \theta,\ z)}\ dz}{\frac{\sin\phi}{r}\ \frac{d\phi}{dr}} \ . \tag{15b}$$

Again note that θ and ϕ are measured at the receiver. Within the limits of our D/h << 1 assumption, r, θ, and R are independent of z and thus

$$N_M(\theta,\phi) = \frac{\left(\frac{P_0}{R}\right)^2 e^{-nR} \int_0^D dz\, N_M(z) \left[\left(1+\alpha^2\right) - 2\alpha \cos\left(2kz\cos\phi_s\right)\right]}{\frac{\sin\phi}{r}\,\frac{d\phi}{dr}}, \tag{16}$$

where

$$\alpha = e^{-k^2\sigma^2\cos^2\phi_s}.$$

The source and receiver angles are related by Snell's law, $\cos\phi_s/c(z_0) = \cos\phi/c(h)$, where c is the fluid phase velocity. Several studies[17,18] have seen an exponential distribution of bubble density with depth. Thus we evaluate the integral in equation (16) for $N(z) = N_0 e^{-z/D}$ after extending the integration limit to $+\infty$. Thus

$$N_M(\theta,\phi) = \frac{N_0 D\left(\frac{P_0}{R}\right)^2 e^{-2nR}\left[\left(1+\alpha^2\right) - \frac{2\alpha}{1+\left(2kD\cos\phi_s\right)^2}\right]}{\frac{\sin\phi}{r}\,\frac{d\phi}{dr}}. \tag{17}$$

It is also instructive to evaluate equation (16) for a uniform distribution of monopoles, $N(z) = N_0$ for $z \le D$ and zero elsewhere. In this case we get

$$N_M(\theta,\phi) = \frac{N_0 D\left(\frac{P_0}{R}\right) e^{-2nR}\left[\left(1+\alpha^2\right) - 2\alpha\frac{\sin\left(2kD\cos\phi_s\right)}{\left(2kD\cos\phi_s\right)}\right]}{\frac{\sin\phi}{r}\,\frac{d\phi}{dr}}. \tag{18}$$

For the case of $\alpha = 1$, equation (18) reduces to the "volumetric source" expression of Bannister, Burgess, and Kewley.[19]

There are numerous physical processes at the sea surface which cause momentum fluctuations[20] that are accurately modeled as surface dipole sources. Analogous with equation (16) we have

$$N_d(\theta,\phi) = \frac{\left(\frac{P_d}{R}\right)^2 e^{-2nR} N_d \cos^2\phi_s}{\frac{\sin\phi}{r}\frac{d\phi}{dr}} , \tag{19}$$

where $N_d P_d^2$ is the dipole source strength per unit surface area.

Before evaluating equations (17), (18), and (19) for arbitrary sound velocity-depth profiles, it is useful to evaluate the equations for a lossless isovelocity ocean, i.e., $c(z) = c$ and $n = 0$. In this case

$$R^2 = r^2 + h^2 = r^2\left(1 + \cot^2\phi\right) = \left(\frac{r}{\sin\phi}\right)^2 ,$$

$$\phi = \phi_s , \text{ and}$$

$$\frac{d\phi}{dr} = \frac{\cos^2\phi}{h} ,$$

and for surface dipoles

$$N_d(\theta,\phi) = N_d P_d^2 \cos\phi . \tag{20}$$

For an exponential distribution of subsurface monopoles we have

$$N_M(\theta,\phi) = N_0 P_0^2 D \frac{\left[\left(1 + \alpha^2\right) - \frac{2\alpha}{1 + (2kD\cos\phi)^2}\right]}{\cos\phi} , \tag{21}$$

and for a uniform distribution of subsurface monopoles we have

$$N_M(\theta,\phi) = N_0 P_0^2 D \frac{\left[\left(1+\alpha^2\right) - 2\alpha \frac{\sin(2kD\cos\phi)}{(2kD\cos\phi)}\right]}{\cos\phi} . \tag{22}$$

As $\phi \to \pi/2$, both equations (21) and (22) become dipole sources with a frequency (wavenumber) dependent strength

$$\lim_{\phi\to\pi/2} N_M(\theta,\phi) = 2N_0 P_0^2 D(2kD)^2 \cos\phi . \tag{23}$$

This result is independent of σ.

It is useful to note that for σ equal to zero

$$\lim_{D\to 0} N_M(\theta,\phi) = 8N_0 P_0^2 R_0^2 k^2 D^3 \cos\phi \qquad \text{(dipole)} \tag{24a}$$

$$\lim_{D\to\infty} N_M(\theta,\phi) = \frac{2N_0 P_0^2 D}{\cos\phi} \qquad \text{(monopole)} \tag{24b}$$

Thus, as the depth of the layer of monopoles becomes small, the directional spectra becomes the same as that due to a "plane" of independent dipoles with a vanishingly small intensity. On the other hand, if the layer becomes deep, then the directional spectra becomes the same as that due to a "plane" of independent monopoles whose intensity increases with the first power of the layer depth.

Thus the shape of the vertical directional spectra changes significantly with the depth of the layer. From equation (16) we see that the directional spectra is a function of the integral of the monopole depth distribution.

Next we are interested in evaluating the directional spectra for an exponentially distributed surface layer of monopoles, equation (17), and a sound velocity-depth profile typical of the experiment conditions considered

later in this report. Over the duration of the experiment, which exceeded 1 year, a wide range of sound velocity-depth profiles existed; however, because the 125-meter receiver depth nearly always exceeded the seasonal thermocline depth, the source-receiver "cross-duct" configuration was typical. In the following calculations we use the sound velocity-depth profile, shown in figure 2, which has a 43-m seasonal thermocline depth. This is not a typical profile but rather is a summer profile. It was chosen because it reduced the computation load of the calculations because the amount of surface contributing to the receiver was limited by refraction. The "limiting ray" at the receiver due to a near-surface source is approximately 95°. Note that in the coordinate system of figure 1, which has the positive z axis pointing down, 0 is down and π is up. Because of the high frequency of the experiment (8 to 64 kHz) we use eikonal equations to model the relevant acoustic propagation and we treat the water column as infinitely deep. This assumption will be justified in the next section. Figure 3 illustrates the dependence of the directional spectra on the depth scale of the exponential layer nondimensionalized by acoustic wavelength. The calculation is performed at 10 kHz (15.5-cm wavelength). The figure illustrates that a thin layer of monopole sources having an exponential length scale exceeding 1 to 2 cm will have a 10 kHz directional spectra observably different from a surface dipole spectra. As the layer thickness increases, the directional spectra moves from a "dipole-like" to a "monopole-like" pattern. This result is a consequence of the directional spectra being due to the independent addition of dipoles (monopole plus negative image) having multiple lobes. The deeper the layer, the more multiple-lobe contributors present, as described by Hallett and Heitmeyer.[21] From figure 3 we conclude that once the exponential length scale exceeds 1 wavelength, the directional spectra is best modeled as a surface layer of independent monopole sources. Experimentally then, the near-horizontally directed acoustic ambient should be a sensitive observation of whether monopole-like or dipole-like behavior exists.

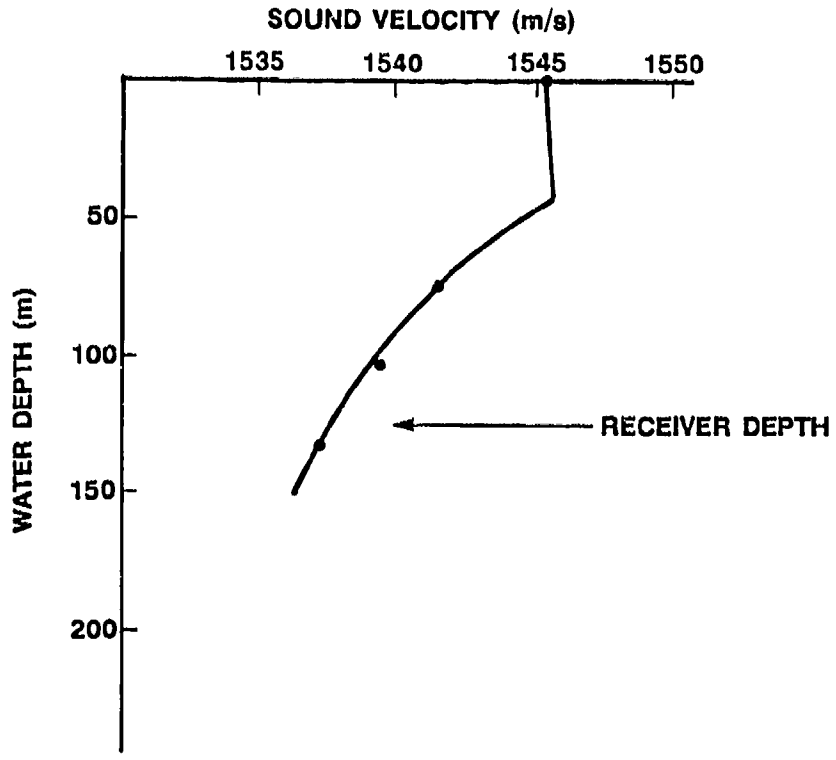

Figure 2. Summer Sound Velocity-Depth Profile

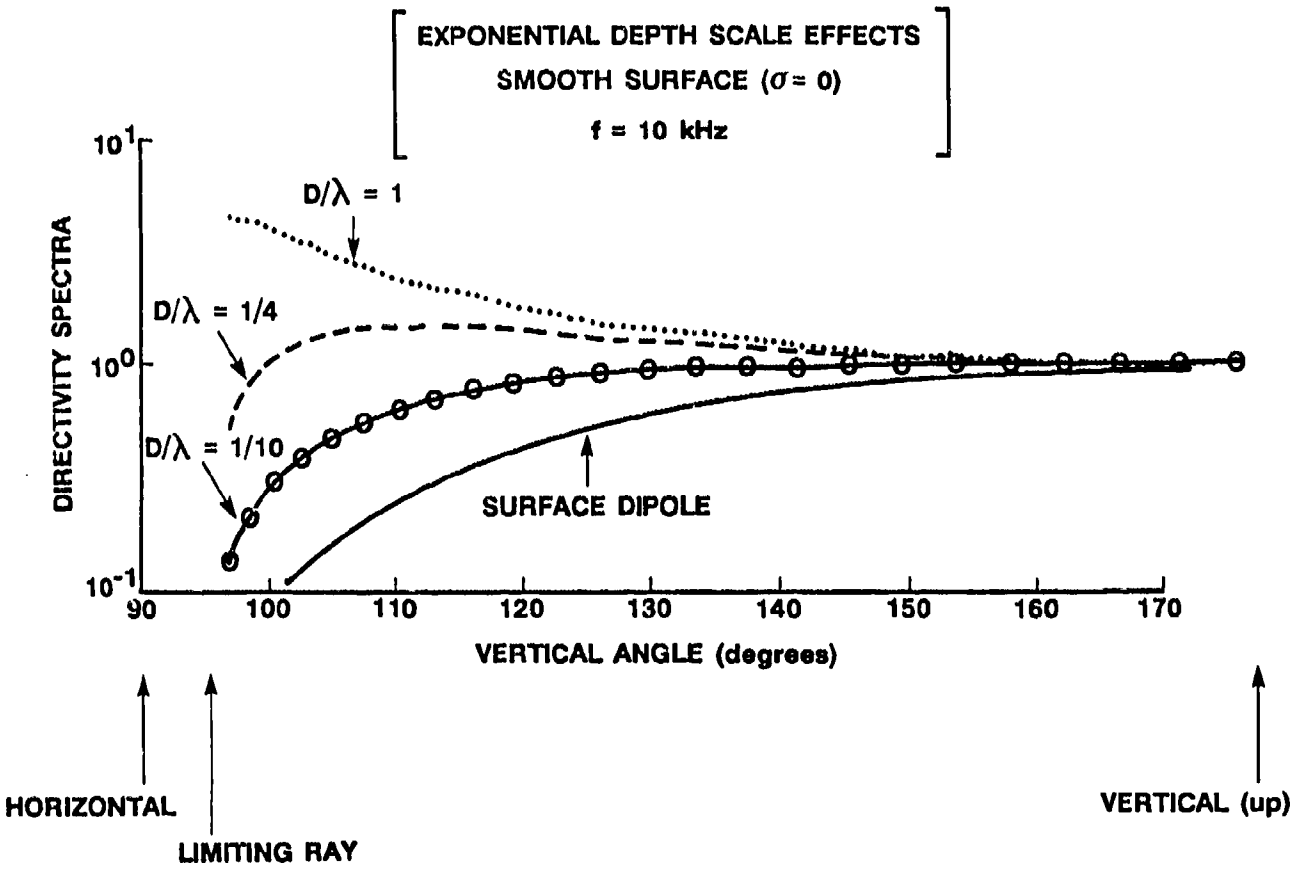

Figure 3. Vertical Directivity Function for an Exponentially Distributed Monopole Subsurface Layer

Figure 3 illustrates the monopole-like behavior of the dipole sources as the separation of the elements of the source and its image becomes a significant fraction of a wavelength even for a perfectly reflecting and flat surface, i.e., an unmodified image source. Figure 4 illustrates that surface roughness also amplifies the monopole-like behavior. Physically this results from a modification of the image source, as would be expected. Figure 5 predicts that with the sound velocity-depth profile of figure 2 the media volume attenuation will also modify the directional spectra at 16 kHz and above. Refractive effects limit the range of the surface contributing to the ambient acoustic field to less than about 2000 meters. Above 16 kHz the attenuation loss beyond that range becomes observable.

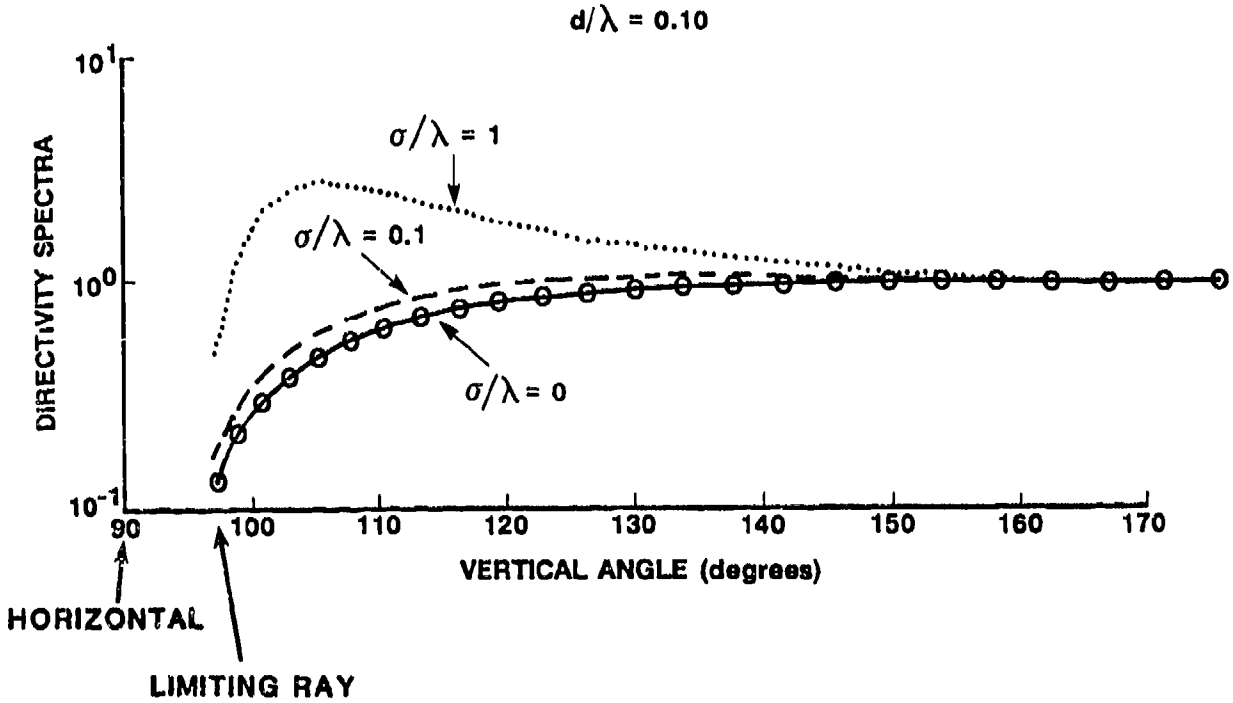

Figure 4. Surface Roughness Effects on the Vertical Directivity Function

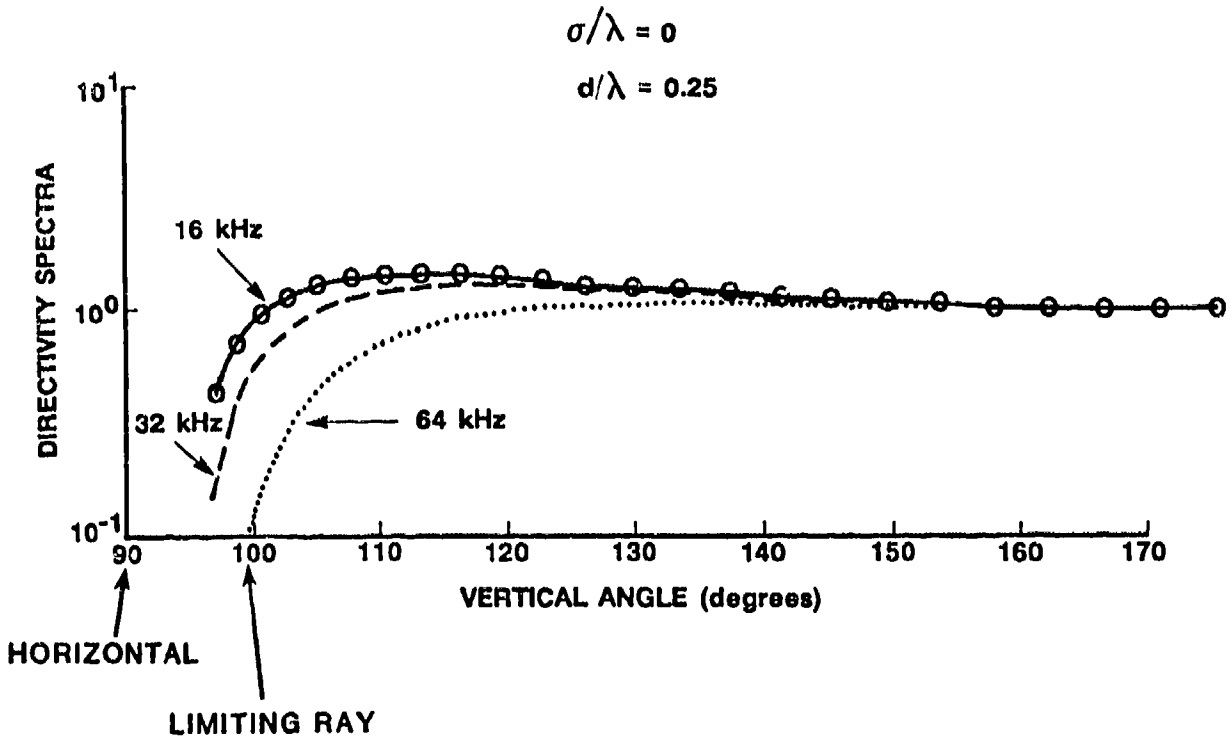

Figure 5. Frequency Effects on the Vertical Directivity Function

3.0 EXPERIMENT DESCRIPTION

3.1 ACOUSTIC DESCRIPTION

Four acoustic sensors were used in this experiment. Three of them were vertical line arrays of hydrophones and the fourth was a single hydrophone. While the latter was certainly the least "directive," it too had some directional characteristics at the higher frequencies measured. The three directional sensors, i.e., line arrays, were internally wired so that only a single output was available from each. This output was the sum of the individual hydrophones of the array, referred to as the "sum beam." The line arrays were approximately 10 wavelengths long at 16, 32, and 64 kHz. The data in this report were taken at 8, 16, 32, and 64 kHz. The 8 and 16 kHz data were taken from the array designated L_1, and the 32 and 64 kHz data were taken from arrays L_2 and L_3. The calculated vertical pattern function for each of these arrays, which contained nonuniform weighting, are pictured in figures 6 through 9. The half-power width of the vertical angular window was approximately 5° at 16, 32, and 64 kHz, and 10° at 8 kHz. The pattern function of each hydrophone in the arrays was azimuthally uniform and mildly nonuniform in elevation angle. The single hydrophone was a composite cylinder having a vertical axis. As was the case with the arrays, the hydrophone had an azimuthally uniform response at all frequencies. In the vertical direction the hydrophone pattern function was mildly directional at 16 kHz and significantly so at 32 and 64 kHz.

Measured patterns exist for the hydrophone. The patterns are rather complex in the "low response" directions but fairly uniform in the "high response" directions. It was useful to model the hydrophone response in such a way that the model fit the "high response" directions well and fit the "low response" directions less well. The requirement of the model was to adequately predict the total hydrophone output in measuring acoustic ambient fields. The model was created by taking the product of a "ring" transducer and a "line" transducer modeled as a zero-order Bessel function and a "sync"

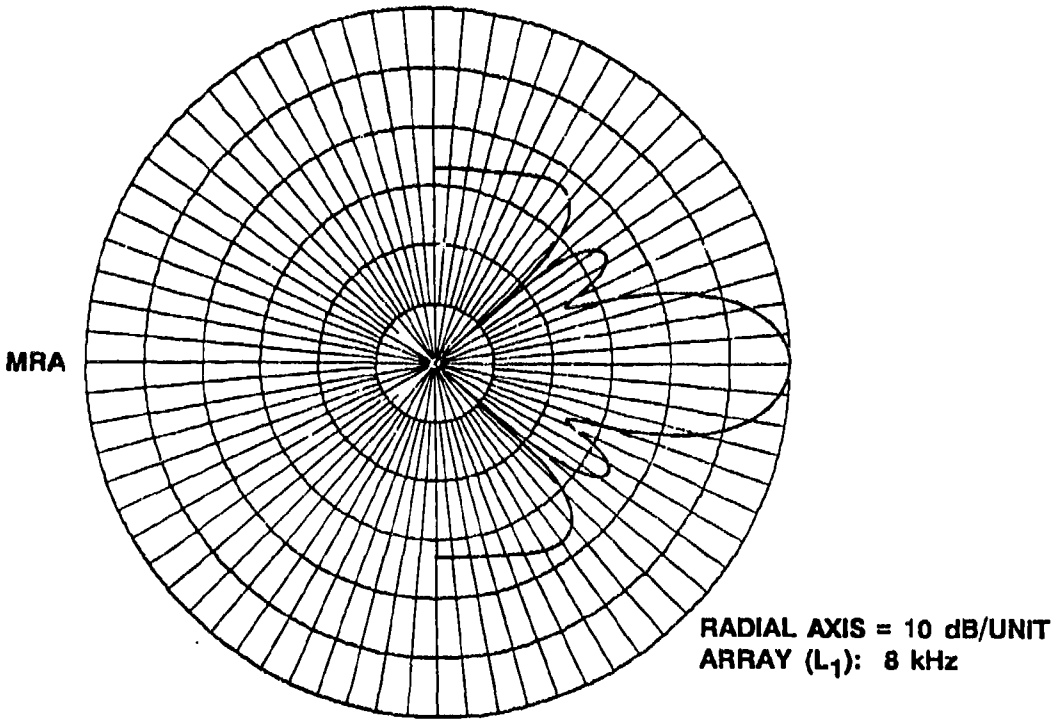

Figure 6. Array L_1 Vertical Pattern Function at 8 kHz

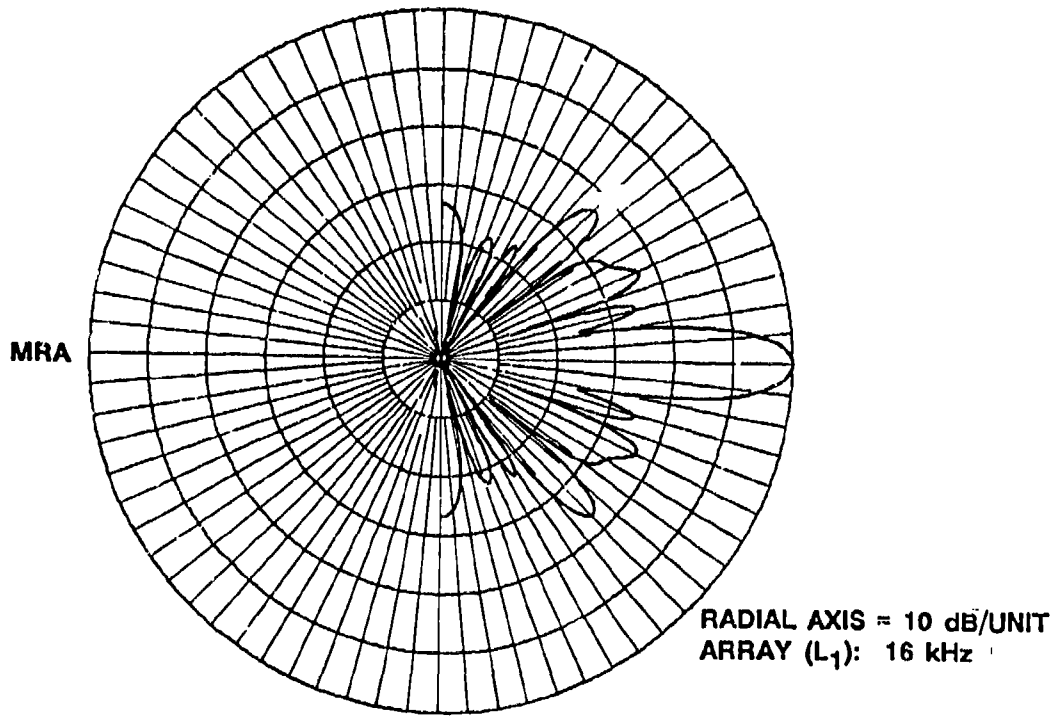

Figure 7. Array L_1 Vertical Pattern Function at 16 kHz

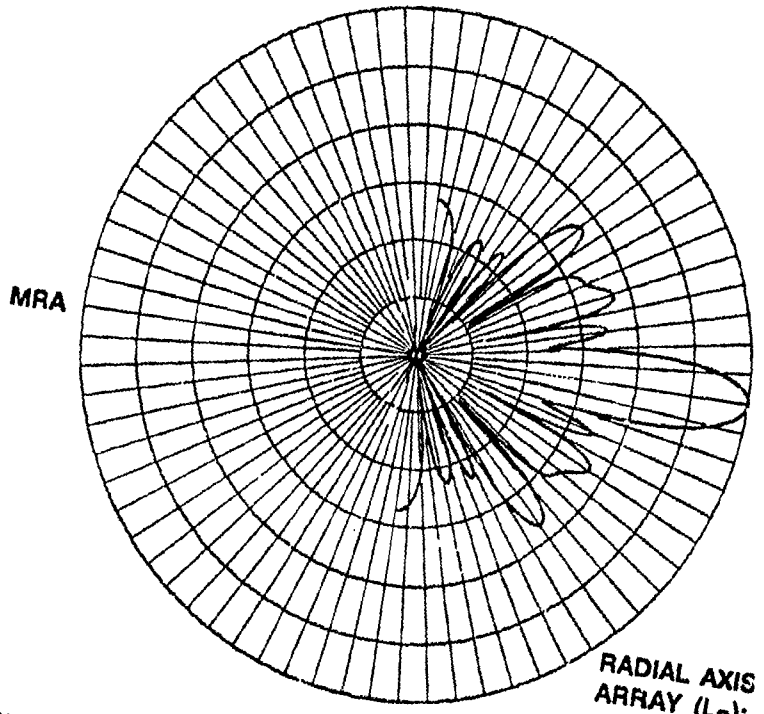

Figure 8. Array L_2 Vertical Pattern Function at 32 kHz

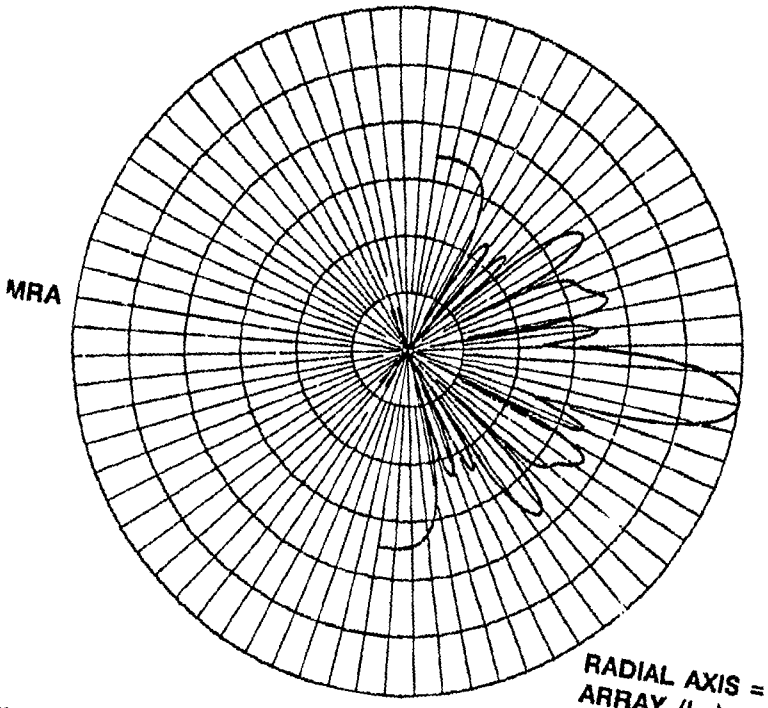

Figure 9. Array L_3 Vertical Pattern Function at 64 kHz

function. The coefficients, i.e., nondimensional cylinder radius and length, were modified to "best" fit the measured patterns. The explicit algorithm is

$$H_2(\phi,f) = J_o\left[\frac{\pi d}{\lambda}\cos\phi\right]\frac{\sin\left[\frac{\pi L \sin\phi}{\lambda}\right]}{\left[\frac{\pi L \sin\phi}{\lambda}\right]}, \tag{25}$$

where J_o is a zero-order Bessel function, ϕ is the elevation angle, λ is the acoustic wavelength, and d and L are the modified cylinder diameter and length scales. Figures 10 through 13 show the calculated hydrophone vertical pattern function at the four frequencies of interest.

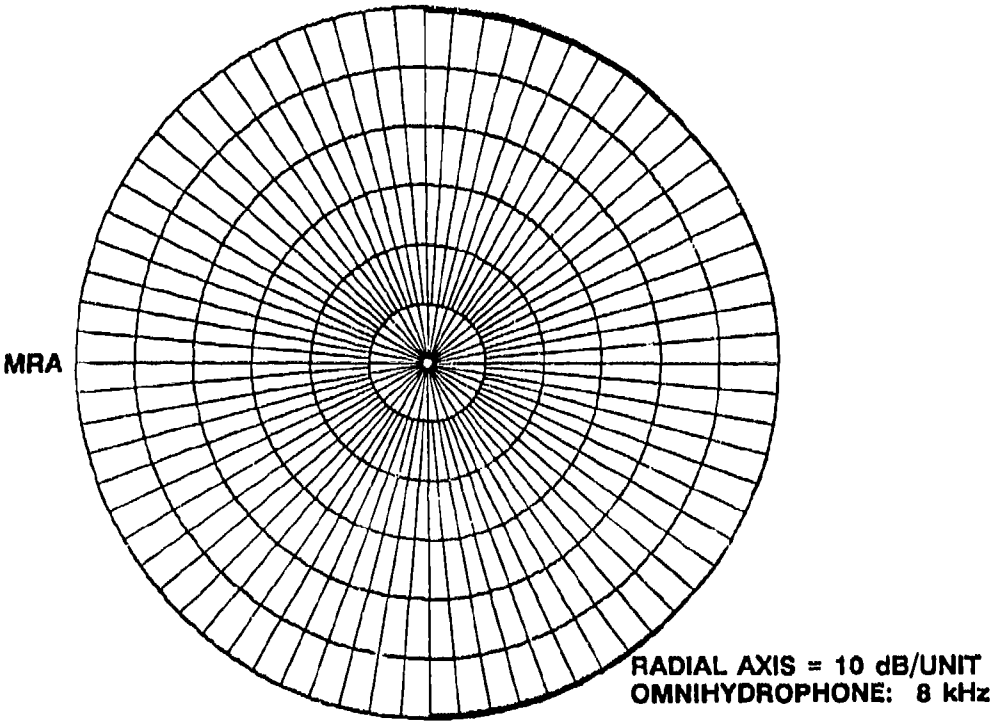

Figure 10. Omnihydrophone Vertical Pattern Function Model at 8 kHz

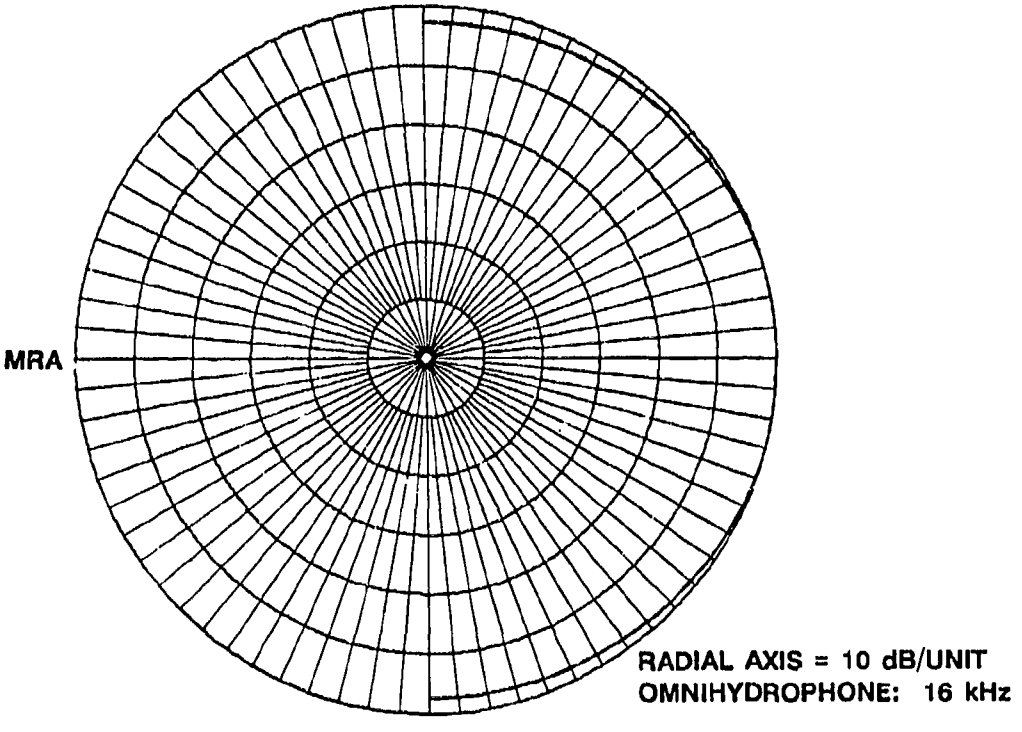

Figure 11. Omnihydrophone Vertical Pattern Function Model at 16 kHz

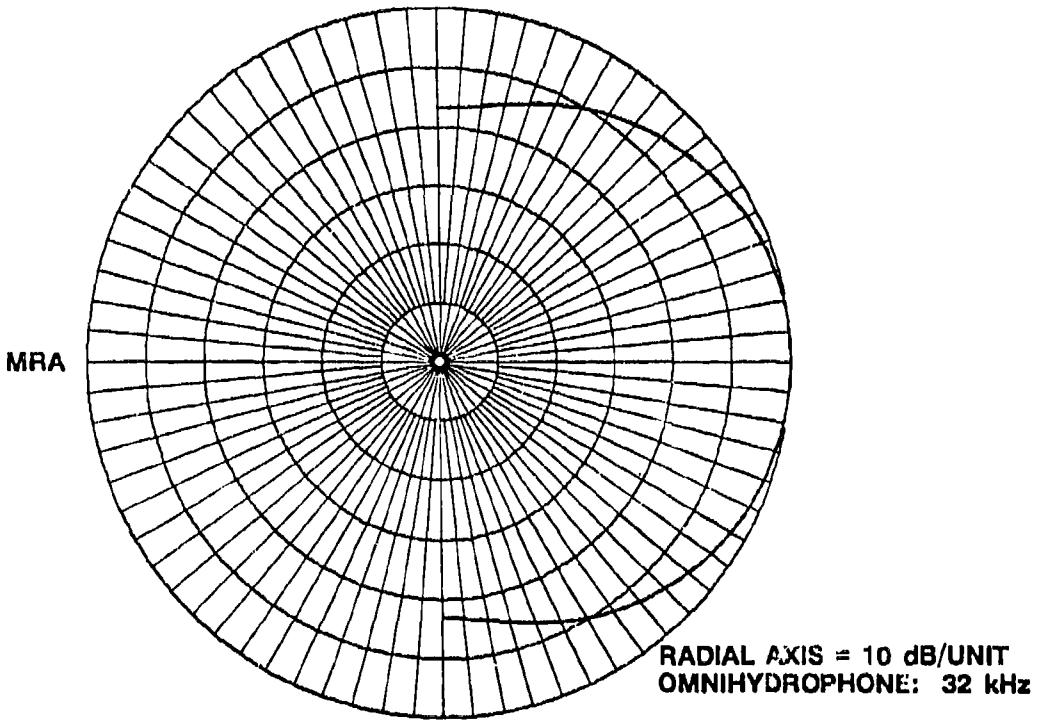

Figure 12. Omnihydrophone Vertical Pattern Function Model at 32 kHz

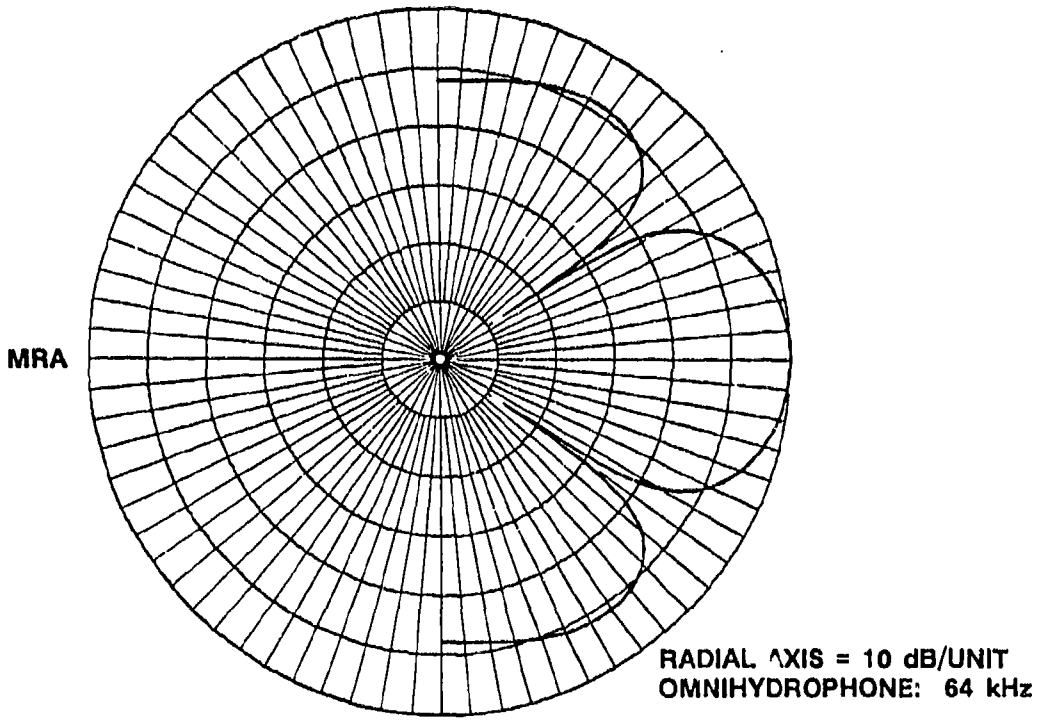

Figure 13. Omnihydrophone Vertical Pattern Function Model at 64 kHz

3.2 EXPERIMENT GEOMETRY

The acoustic sensors were located in The Tongue of the Ocean (TOTO), The Bahamas. They were positioned in the middle of the major axis of the tongue at a latitude of 24°40′ N. The sensors were at a depth of 125 m in water 1830 m deep. The location was approximately 12 km from the nearest escarpment. If we define a "range curtain" to be the range at which the geometric spreading loss is matched by the attenuation loss, then the maximum range of influence was less than 35 km for frequencies greater than 8 kHz. All data were examined for signs of extraneous acoustic signals, and all suspect data sets were discarded.

The four sensors were moored to the bottom, and each of the sensors was electrically hard wired to the AUTEC, Andros Island Site 1 facility for recording and analysis. Data were available from 20 May 1988 to 3 April 1989. During that period 215 data sets of appropriate quality became available for this analysis. The approximate 1-year period of the experiment sampled all seasons of the local sound velocity-depth profile shown in figure 14. The 125-m depth of the sensors means that, aside from the short period for which the winter profile existed, the measurements were made beneath the seasonal thermocline.

3.3 DATA ANALYSIS

The analysis described in section 2 treats a "bottomless" ocean, i.e., only down-going acoustic propagation is possible. To check the conformity of this approach with the realities of the experiment, the directional spectra were estimated using the techniques described by Kennedy and Szlyk in 1988.[22] The approach features a propagation loss algorithm that obtains full solutions of the acoustic wave equation, surface roughness, arbitrary sound velocity-depth profiles, arbitrary bottom geoacoustic parameterizations, and a plane of independent dipole radiators located on the water surface. An important weakness of the approach is that it ignores all range dependency. In the geometry of this experiment, range-dependent bathymetry is an issue. Thus the prediction ignores steep-to-shallow angle direction conversion that might occur at

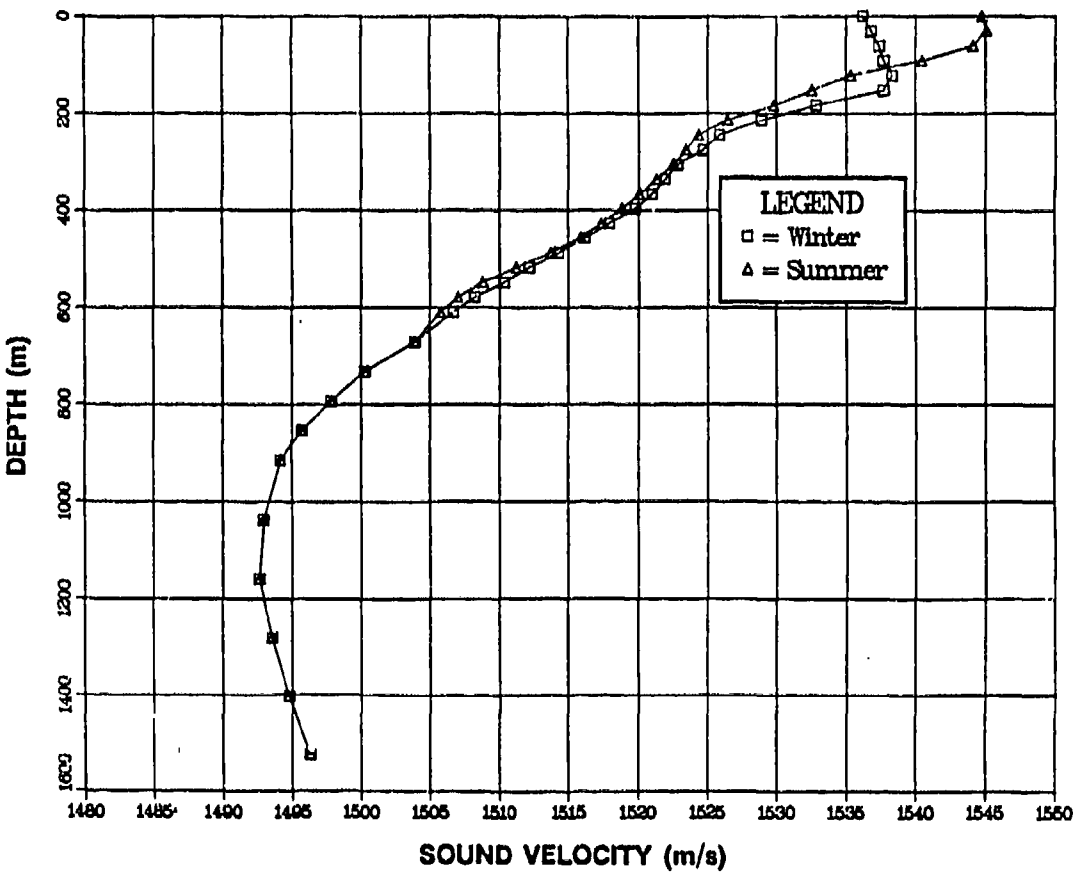

Figure 14. Sound Velocity-Depth Profile of TOTO

the escarpments. The results of the calculations are shown in figures 15 and 16 which illustrate the predictions for summer and winter profiles, i.e., characterized by the depth of the seasonal thermocline (figure 14). The specific bottom loss characterization used for the 8 through 64 kHz frequency range is from Marsh and Schulkin.[23] The figures indicate the reflected bottom energy in this frequency range is in excess of 15 dB less than the direct energy. The conclusion is that a bottomless ocean is a reasonable model.

The autospectral density of each of the four sensors was determined using constant-bandwidth Fourier transform analysis techniques. The spectral resolution of the measurements using a Hanning window was 15, 37.5, and 75 Hz for the three analysis ranges. Fifty nonoverlapped transforms were averaged to estimate the spectral density. The confidence interval of these spectral estimates is $\pm$1.1 dB. The spectral estimates were compared with anticipated electronic noise limitations. This was not a straightforward operation because full system electronic noise "floors" were not readily obtained; however, any data failing to meet the anticipated voltage limitations were discarded. The autospectral density values from each of the sensors at 8, 16, 32, and 64 kHz were then manually recorded.

The line antenna array gain was evaluated by taking the ratio of the line array output to the hydrophone output. The array gain was then compared with a calculated directivity index, to be described shortly, and the difference, which was labeled anisotropic gain, was recorded in a data base that contained wind speed measurements made at the time of the array output measurement. The hydrophone autospectral density was also included in the data base. The anemometer used was located 10 m above the sea surface on a small tower located in the shallows adjacent to Andros Island. The anemometer was approximately 13 km from the acoustic sensor location. The data base was accumulated on a mainframe computer which then was used to generate the results described in the next section of this report.

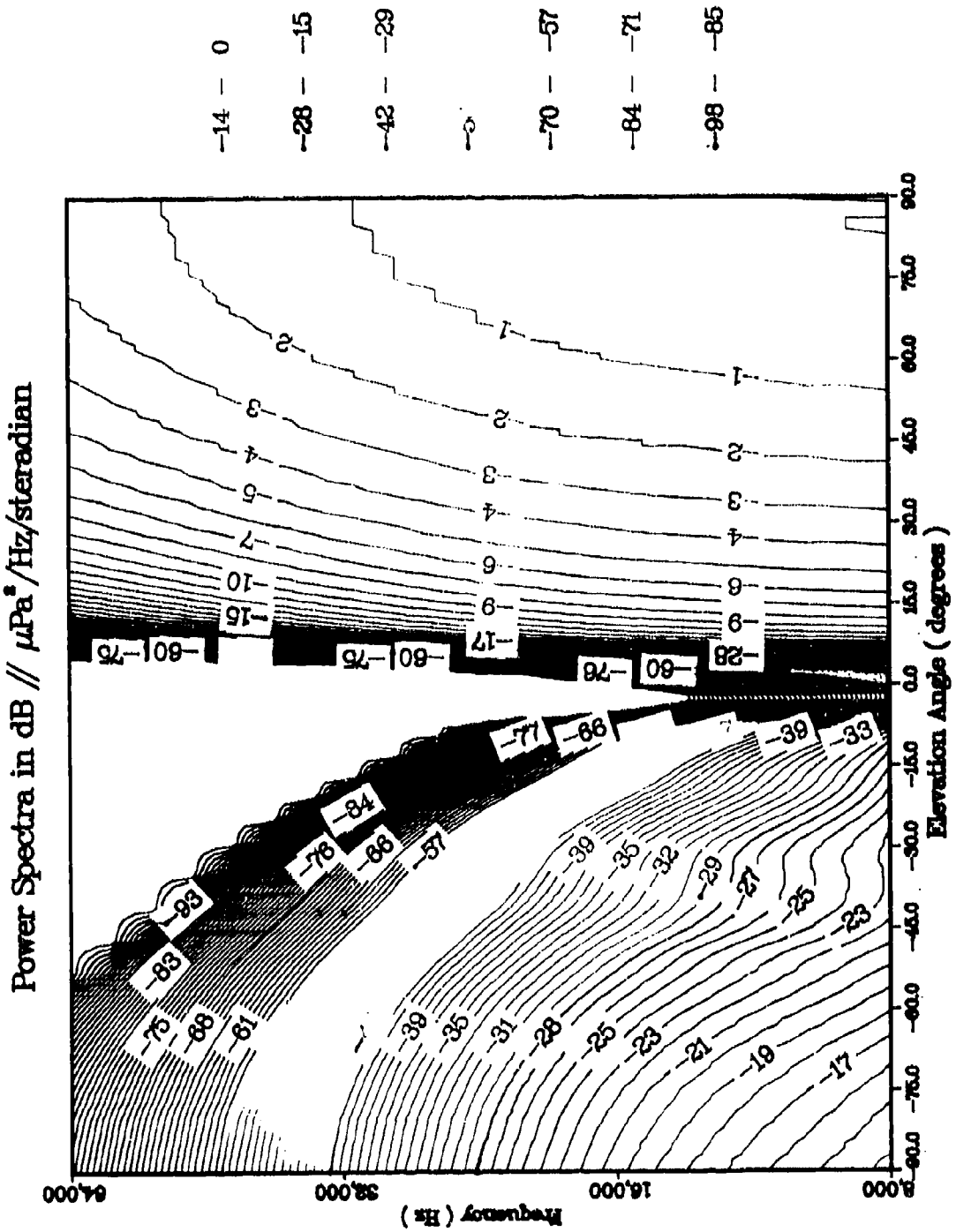

Figure 15. Frequency-Directivity Spectra for a Summer Dipole Noise Model

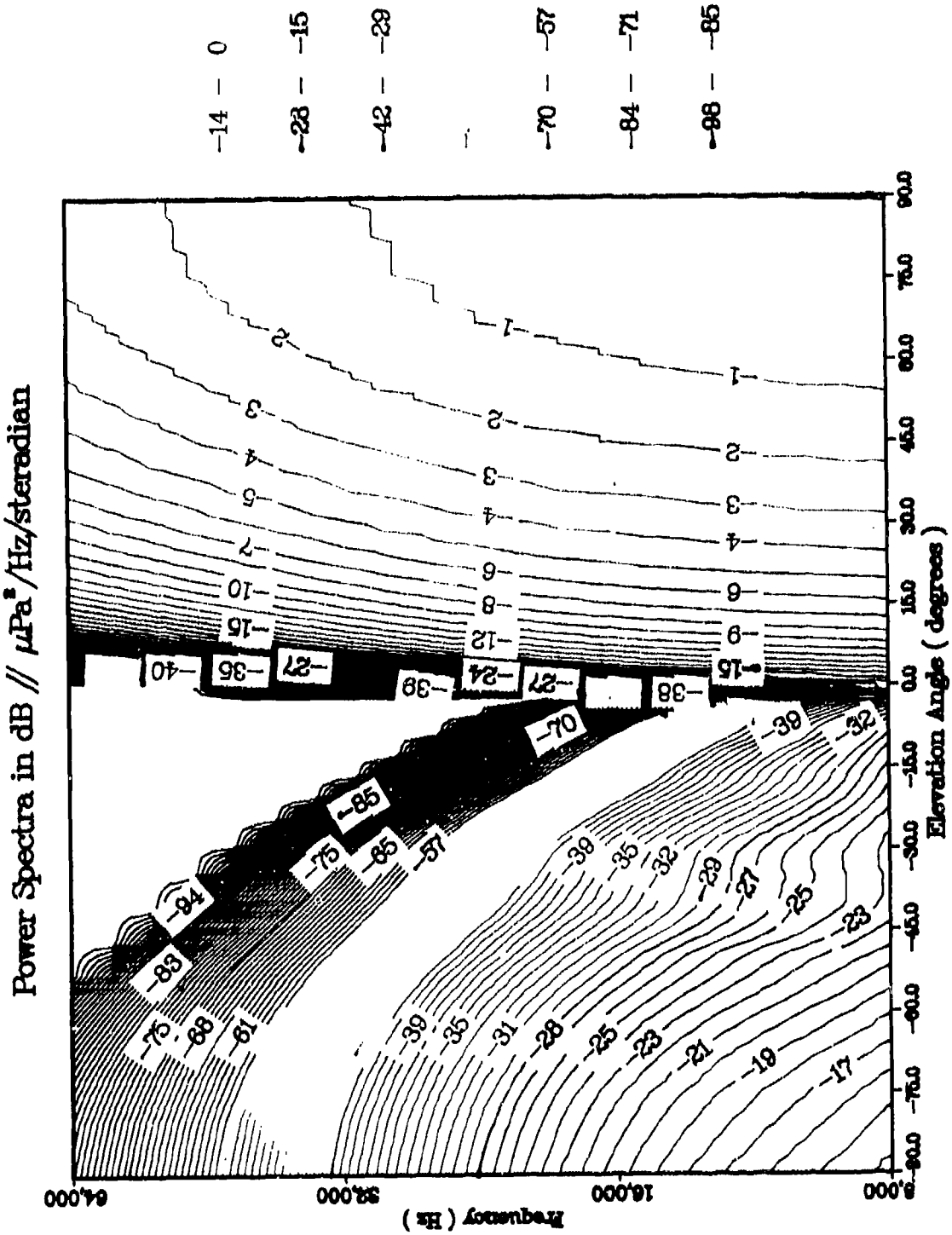

Figure 16. Frequency-Directivity Spectra for a Winter Dipole Noise Model

The directivity index that served as the reference for the hydrophone line array outputs was calculated so that it represented the directivity index of the measurement hardware. Thus all the acoustic antenna results were normalized by the directivity index, which was found by calculating the ratio of the outputs of each of the three arrays to the output of the reference hydrophone, all in the presence of a three-dimensional isotropic pressure field. The calculation was made using the equation

$$DI = \frac{\int_0^{\pi} B(\phi,f)H_1(\phi,f)\ \sin\phi\ d\phi}{\int_0^{\pi} H_2(\phi,f)\ \sin\phi\ d\phi}\ , \tag{26}$$

where $B(\phi,f)$ is the pattern function of the appropriately weighted and spaced "point" hydrophones, $H_1(\phi,f)$ is the pattern function of the individual hydrophones used in the antennas, and $H_2(\phi,f)$ is the directional pattern of the hydrophone calculated in equation (25). Correcting measured data to account for sensor pattern functions is traditionally difficult because the data represent the integral of the product of the pattern function and the solid angle density function of the field variable being measured. Thus the experimenter is in the dilemma of needing the result of the measurement prior to making the correction. This was avoided here by not "correcting" the array gain measurement but rather by comparing it with the directivity index which, by definition, assumes an explicit solid-angle density function. However, in presenting the hydrophone output as a measure of the total acoustic intensity, it is necessary to make a correction for the transducer vertical pattern function. We will make the correction by letting $S_h(\omega)$ be hydrophone (measured) autospectral density

$$S_h(\omega) = \int_{4\pi} d\psi\ H_2(\omega,\psi)N(\omega,\psi)\ , \tag{27}$$

where ψ is the solid angle, H_2 is the hydrophone pattern function, and N is the actual noise field directional function. An omnidirectional hydrophone would measure

$$S_o(\omega) = \int_{4\pi} d\psi \; N(\omega,\psi) \quad . \tag{28}$$

Forming the ratio

$$\frac{S_h(\omega)}{S_o(\omega)} = \frac{\int_{4\pi} d\psi \; H_2(\omega,\psi) N(\omega,\psi)}{\int_{4\pi} d\psi \; N(\omega,\psi)} \tag{29}$$

requires an explicit form for $N(\omega,\psi)$. Following Cox,[24] we expand the directional spectra in terms of Legendre polynomials, $P_n(\cos\phi)$, after asserting azimuthal symmetry of the pressure field. The result is

$$N(\omega,\phi) = \sum_{n=0}^{\infty} c_n(\omega) P_n(\cos\phi) \quad . \tag{30}$$

The advantage of this form is that the field is expressed as perturbations ($n > 0$) on an isotropic field ($n = 0$). This follows from

$$P_0(\cos\phi) = 1 \quad . \tag{31}$$

In correcting for the hydrophone pattern function in our measurements we limit ourselves to a first-order isotropic approximation so that

$$S_o(\omega) = S_h(\omega) \frac{\int_0^{\pi} \sin\phi \; d\phi}{\int_0^{\pi} \sin\phi \; d\phi \; H_2(\omega,\phi)} \quad . \tag{32}$$

Attention needs to be drawn to the "hole" in the directivity spectra (at $\phi = \pi/2$) that is predicted when the receiving hydrophones are below the seasonal thermocline. This "hole" is seen in figure 15, as well as in figures

3 through 5. The sound velocity-depth profile used to generate these figures used a fast surface velocity (1545 m/s) which maximized the size of the "hole." In general the size of "hole," relative to the size of the half-power beamwidth, is frequency and sound velocity dependent, so the frequency variation of a beamformer output would be expected to decrease as the frequency increases to the point that the beampattern half-power beamwidth becomes narrower than the "hole." The beamformer output usually decreased at approximately the 3 dB per octave rate one would expect without the "hole" present. Thus the "hole" was not identified in the data.

The two fundamentally independent variables of the experiment are wind speed and frequency. The measured wind speed at a 10-m height is better related to "sea surface sound" by converting the measurement to friction velocity (U_*), i.e., atmospheric stress on the ocean surface, as done by Kerman.[7] The published algorithm of Wu[25] was used to make the conversion. Friction velocity will be presented in a nondimensional form by normalizing the minimum phase velocity (U_0) of the capillary-gravity wave field.[7] A unity value of the nondimensional friction velocity will be used as the point of incipient whitecapping.

4.0 EXPERIMENT RESULTS

4.1 ACOUSTIC INTENSITY

The hydrophone autospectral densities are displayed as a function of wind speed in figures 17 through 20. These data are compared with previous measurements to establish a historical relation. All data sets are compared with the well-known globally averaged Knudsen curves.[2] In addition, the 8 and 16 kHz data could be compared with the Caron and Sheffield data.[26] The latter data were taken in the same area some years earlier. One sees that the present data are consistent with the Caron and Sheffield data, as they should be, and are similar to but consistently lower than the Knudsen data except at 64 kHz. The lack of predicted wind speed dependence in the 64 kHz data is unexpected, and it can only be assumed that the sensor was not operating correctly at that frequency, possibly because of an undetected electronic noise limitation. No further analysis of the 64 kHz data was undertaken.

Figure 21 illustrates the frequency dependence of the data. The figure was determined by grouping the data into the wind speed cells shown in the figure at each of the selected frequencies. A regression line was than fit across the frequency to each wind speed cell. The resulting "power law" fit to the data indicated a frequency dependence that varied from -1.74 at the lowest wind speed cell to -2.1 at the highest wind speed cell. The slopes are comparable with the "classical" 5 to 6 dB/octave, i.e., -1.7 to -2.0, associated with the Knudsen curves. These same slopes are obtained from physical arguments. Measured acoustic spectra[27] due to spray on the surface is -1.7. A -2 dependence was obtained by Prosperetti on purely theoretical grounds when modeling the acoustic radiation of oscillating bubbles resulting from a whitecap.[28]

The previous hydrophone sound pressure level data were replotted as a function of nondimensional friction velocity, i.e., surface friction velocity nondimensionalized by the minimum phase speed of the capillary-gravity wave.

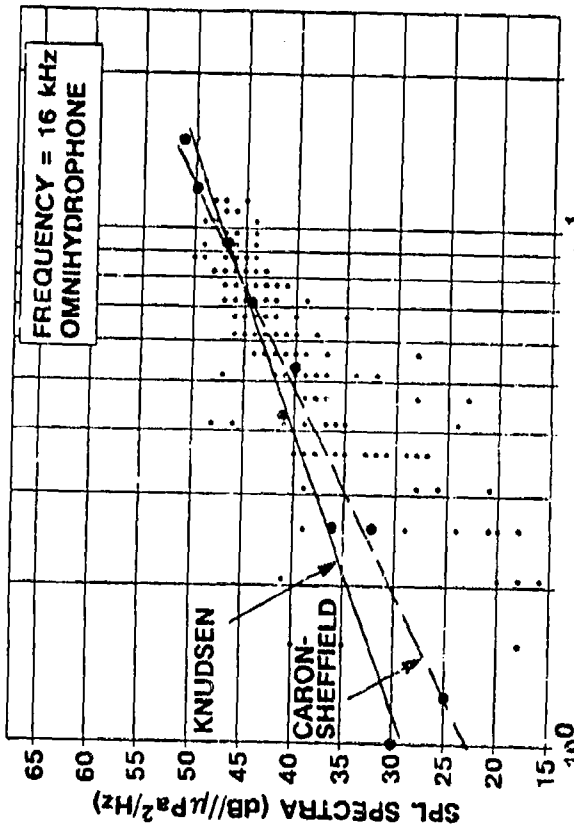

Figure 18. Omnihydrophone SPL Versus Wind Speed at 16 kHz

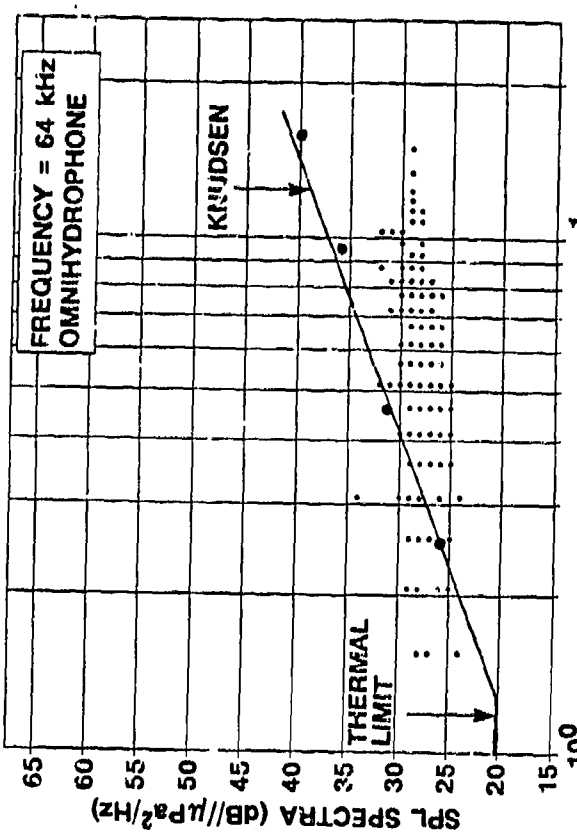

Figure 20. Omnihydrophone SPL Versus Wind Speed at 64 kHz

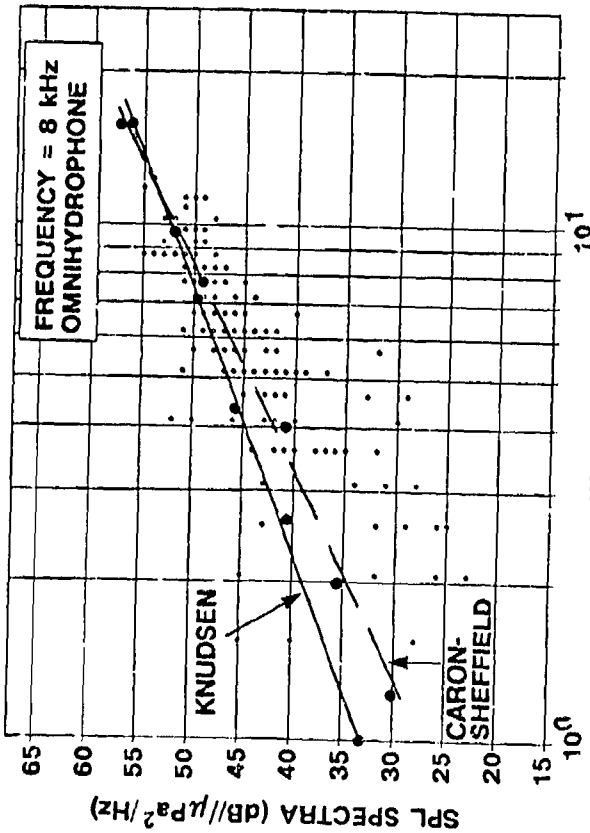

Figure 17. Omnihydrophone SPL Versus Wind Speed at 8 kHz

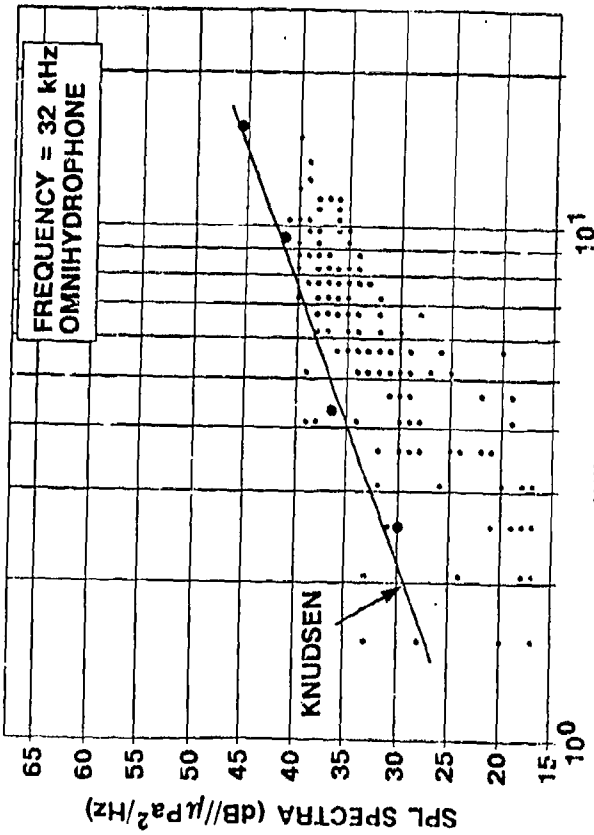

Figure 19. Omnihydrophone SPL Versus Wind Speed at 32 kHz

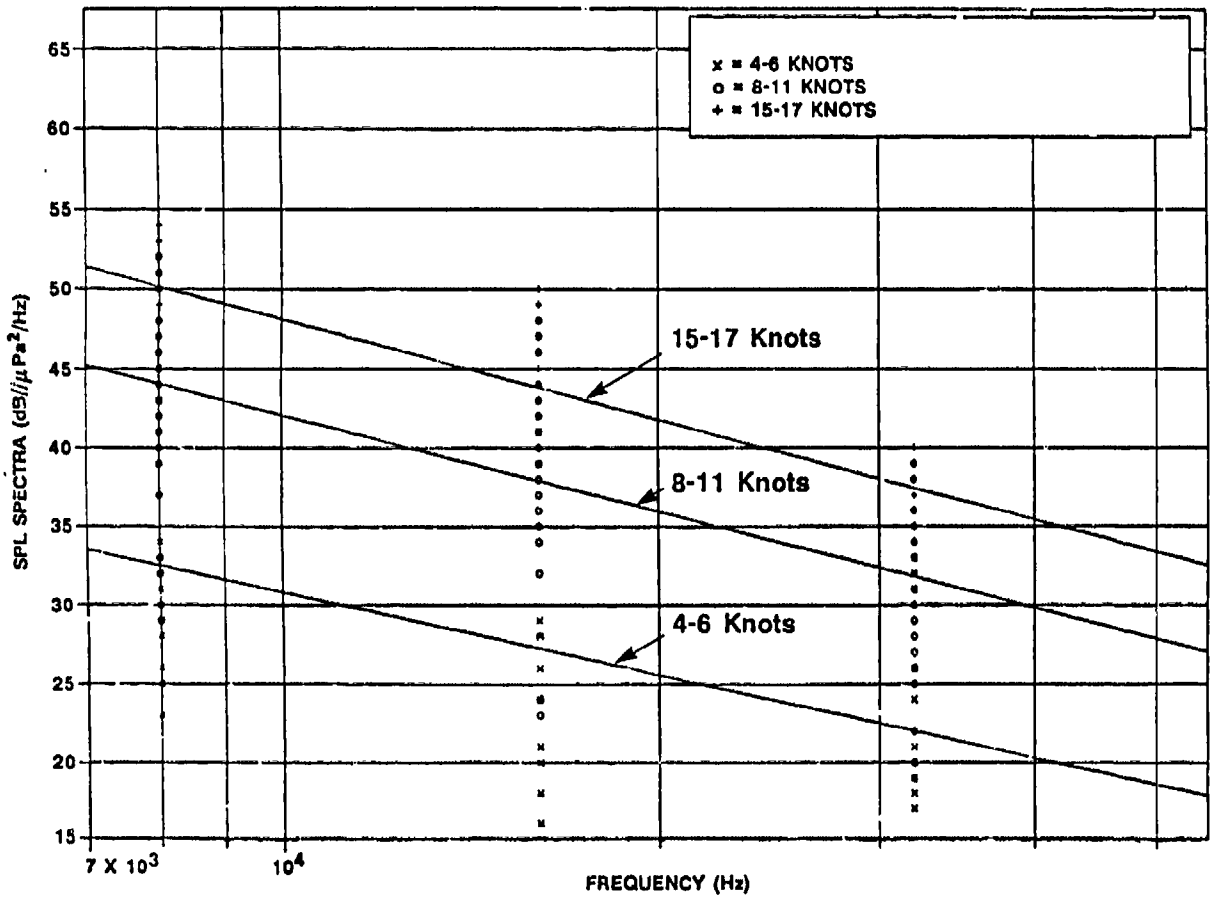

Figure 21. Frequency Dependence of SPL Data at Various Wind Speeds

The traditional idea is that a value of 1 for this nondimensional variable represents incipient whitecapping. Each of the data sets is partitioned into "whitecaps present" (WP) and "whitecaps not present" (WNP) according to whether the nondimensional friction velocity is greater than or less than 1, respectively. A regression line is fit to each partition. The results for each frequency are presented in figures 22 through 24. The slope of the line is seen to be different for the WP and WNP cases. For the WP case the power law exponent varies from 2.2 to 2.9. For the WNP case the exponent varies from 1.2 to 1.9. A composite of all of the data is obtained by adjusting the curves so that the center of mass of the data at a nondimensional friction velocity of 1 coincides. This is illustrated in figure 25. The resulting power law fit to the composite data yields 2.5 and 1.6 respectively for the WNP and WP cases. This is a somewhat smaller exponent for the WNP case than the 3.0 reported by Kerman.[7] However, for the WP case the agreement is quite good, i.e., 1.5 vice 1.6. There appears to be no physical argument for either power law. One obvious characteristic of the data being presented is the larger variability of the WNP data relative to the WP data. This observation is quantified in figures 26 and 27 which are histograms of the residuals plotted to the regression lines of figure 25 for the WNP and WP cases. The difference is striking.

4.2 ANISOTROPIC ARRAY GAIN

We explicitly defined a term in section 3.3, i.e., anisotropic array gain, to describe the difference in the realized gain of the array relative to the directivity index of the array. By array gain we mean the improvement in signal-to-noise ratio (SNR) between the SNR of the homogeneous pressure field measured by the array's hydrophones and the array beamformer output when "steered" to the horizontal direction. Array gain is measured here without a signal field present by "calibrating" the beamformer output so that its response to an acoustic plane wave arriving from the "steered" direction is at the same acoustic level as seen by the hydrophone. In this case, which is typical of the industry, the signal gain is unity and the measured

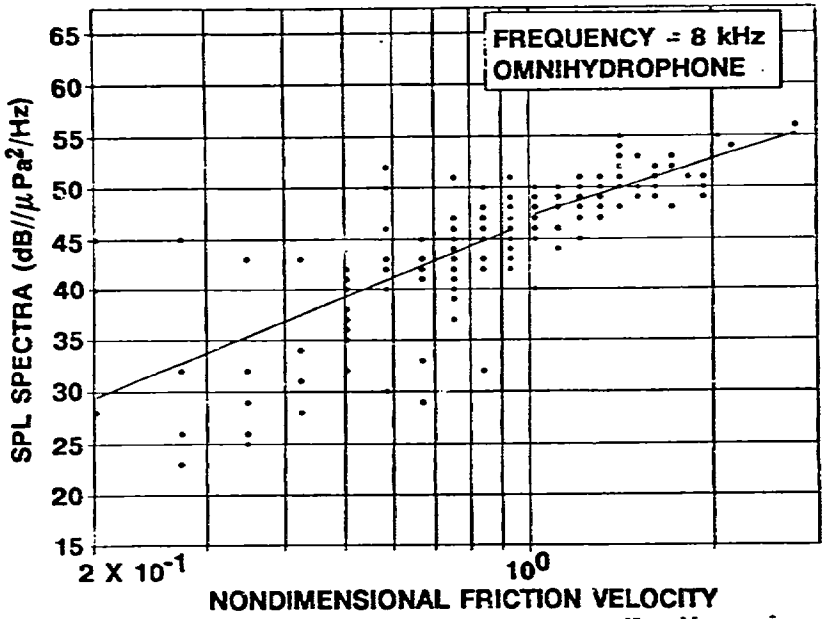

Figure 22. Omnihydrophone SPL Versus Nondimensional Friction Velocity at 8 kHz

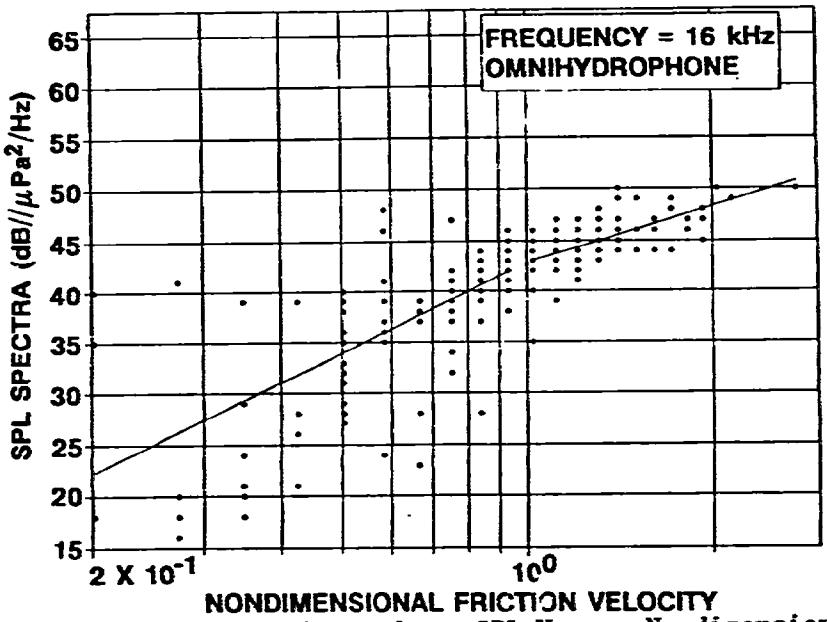

Figure 23. Omnihydrophone SPL Versus Nondimensional Friction Velocity at 16 kHz

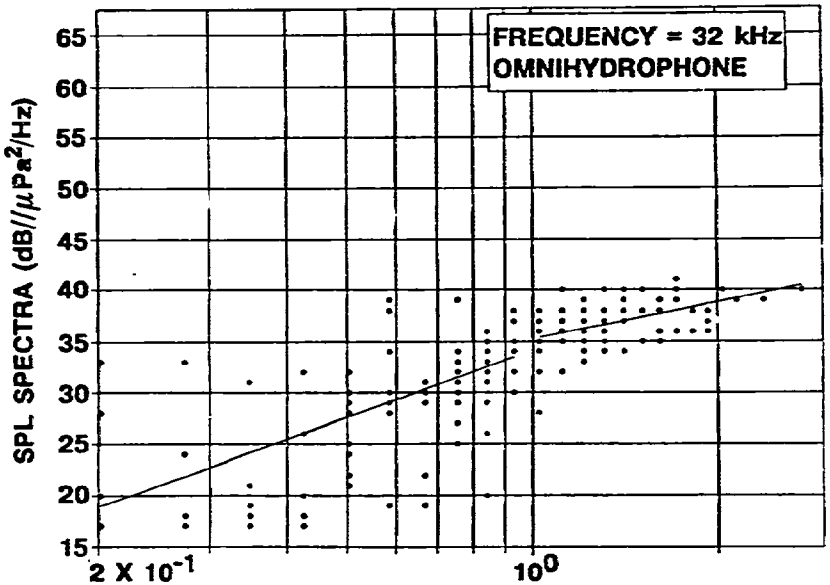

Figure 24. Omnihydrophone SPL Versus Nondimensional Friction Velocity at 32 kHz

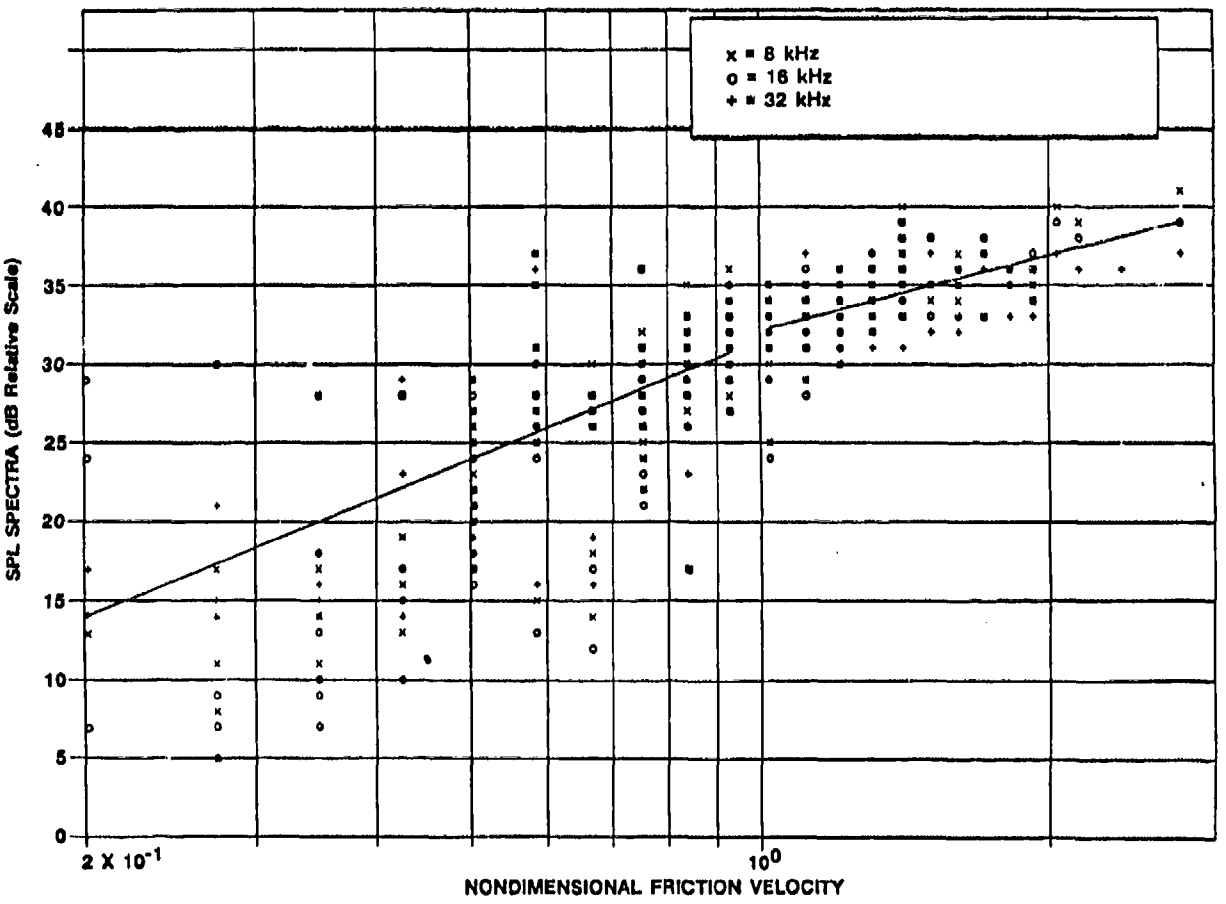

Figure 25. Composite SPL Versus Nondimensional Friction Velocity

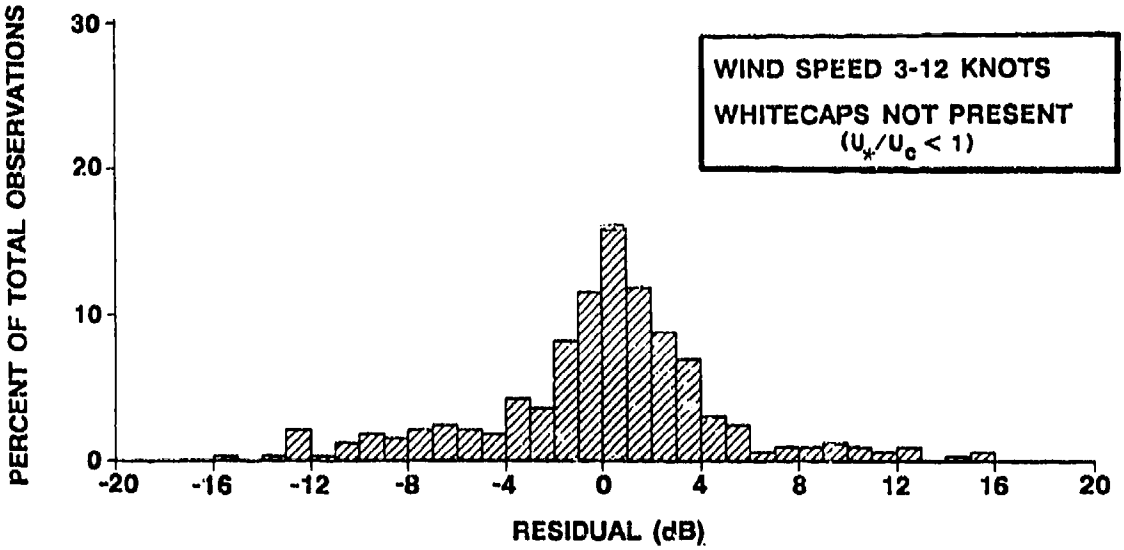

Figure 26. Histogram of Residuals in SPL Data With Whitecaps Not Present

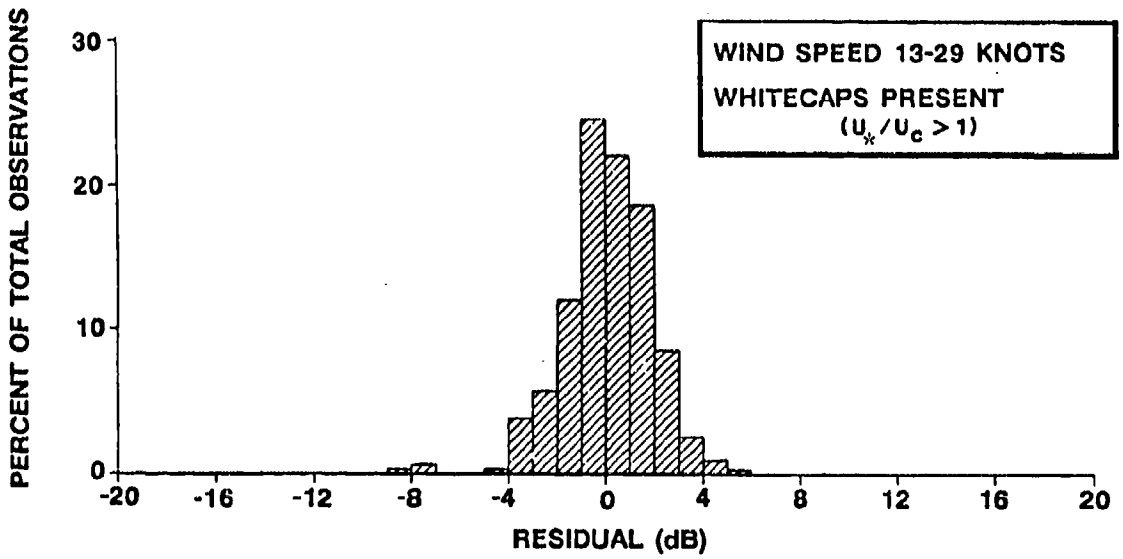

Figure 27. Histogram of Residuals in SPL Data With Whitecaps Present

noise reduction is exactly the reciprocal of the array gain. We then calculated a term which we call the anisotropic array gain which measures the array gain due to the presence of vertical anisotropy in the acoustic ambient field by normalizing the measured array gain by a calculated directivity index (equation (26)).

Figures 28 through 30 show that the anisotropic gain, when "steered" to the horizontal direction, is significantly wind speed dependent. In general the gain exceeds that of an isotropic noise field at high wind speeds and is less than the isotropic gain at low wind speeds. The frequency dependence of these observations is shown in figure 31, which illustrates a mild frequency variation. The functional fit to the data, grouped by wind speed, is a second-order polynomial regression. The 16 kHz peaking appears to be physically significant. To examine this wind speed dependence, we again use the nondimensional friction velocity as the independent variable in figures 32 through 34. As was the case for the acoustic intensity, there is a clear change in the character of the curve for unity value of the independent variable, indicating a physical process change between the whitecaps present case and the whitecaps not present case. A nondimensional anistropic gain was formed by equating the center of mass of the data for each frequency at a nondimensional friction velocity of 1. This nondimensional data composite is shown in figure 35. Each data set was again subdivided into the two cases and a power law was fit to each subset. In the WNP case the individual power varied from 1.6 to 2.1, with the composite value being 1.9. In the WP case the individual powers varied from 0.04 to 0.12, with the composite being 0.1. Thus the array gain in the horizontal direction is nearly independent of wind speed if whitecaps are present and changes at some 19 dB per decade if whitecaps are not present.

As was true for the acoustic intensity, the spread of the residuals about the regression line fit is noticeably different between the WNP and WP cases. This is shown clearly in figures 36 and 37, which are histograms of the residuals in each case. However, what is unique to the anisotropic gain case is the nonsymmetric distribution of the WP case histogram. This visually apparent characteristic of the data was checked by calculating a measure of

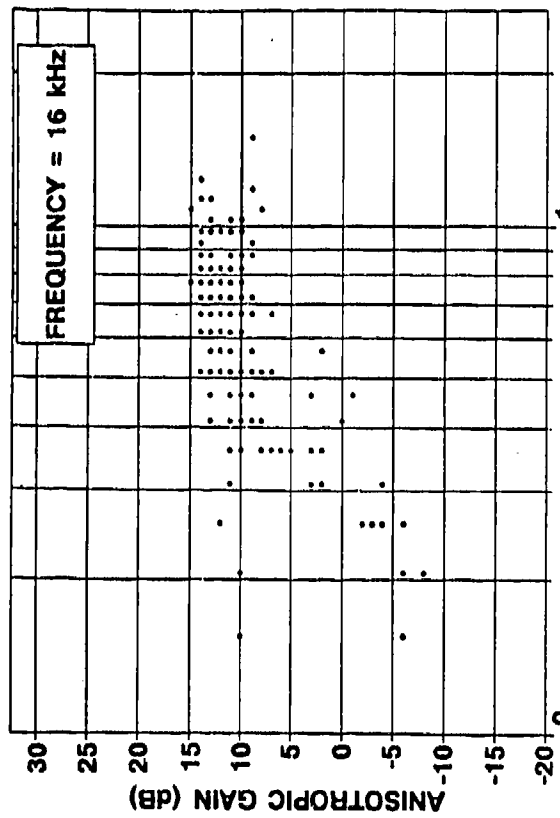

Figure 29. Anisotropic Gain Versus Wind Speed at 16 kHz

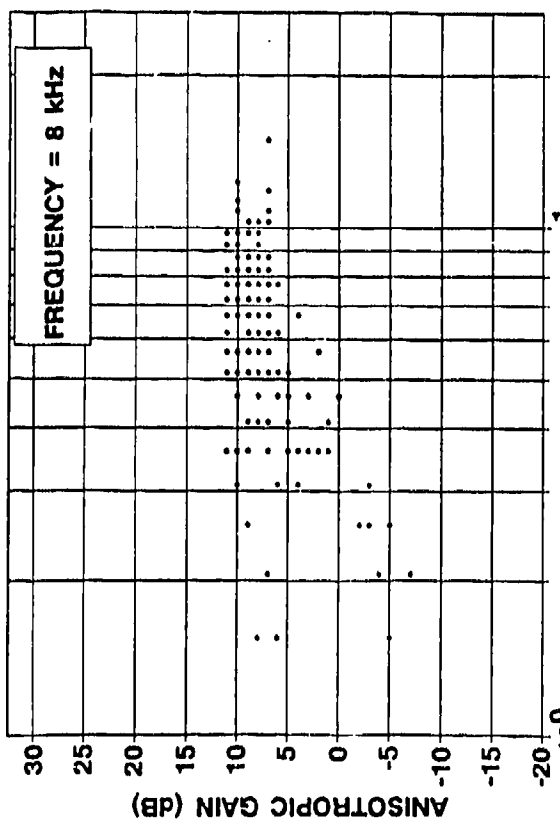

Figure 28. Anisotropic Gain Versus Wind Speed at 8 kHz

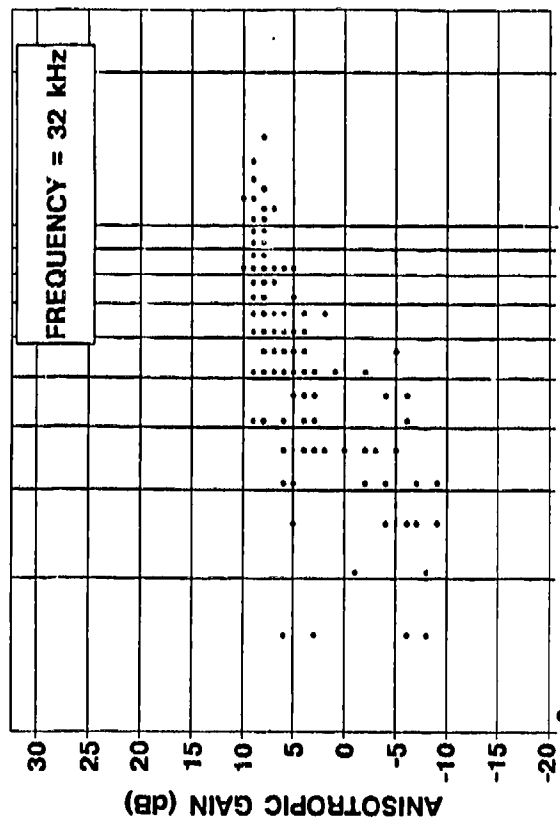

Figure 30. Anisotropic Gain Versus Wind Speed at 32 kHz

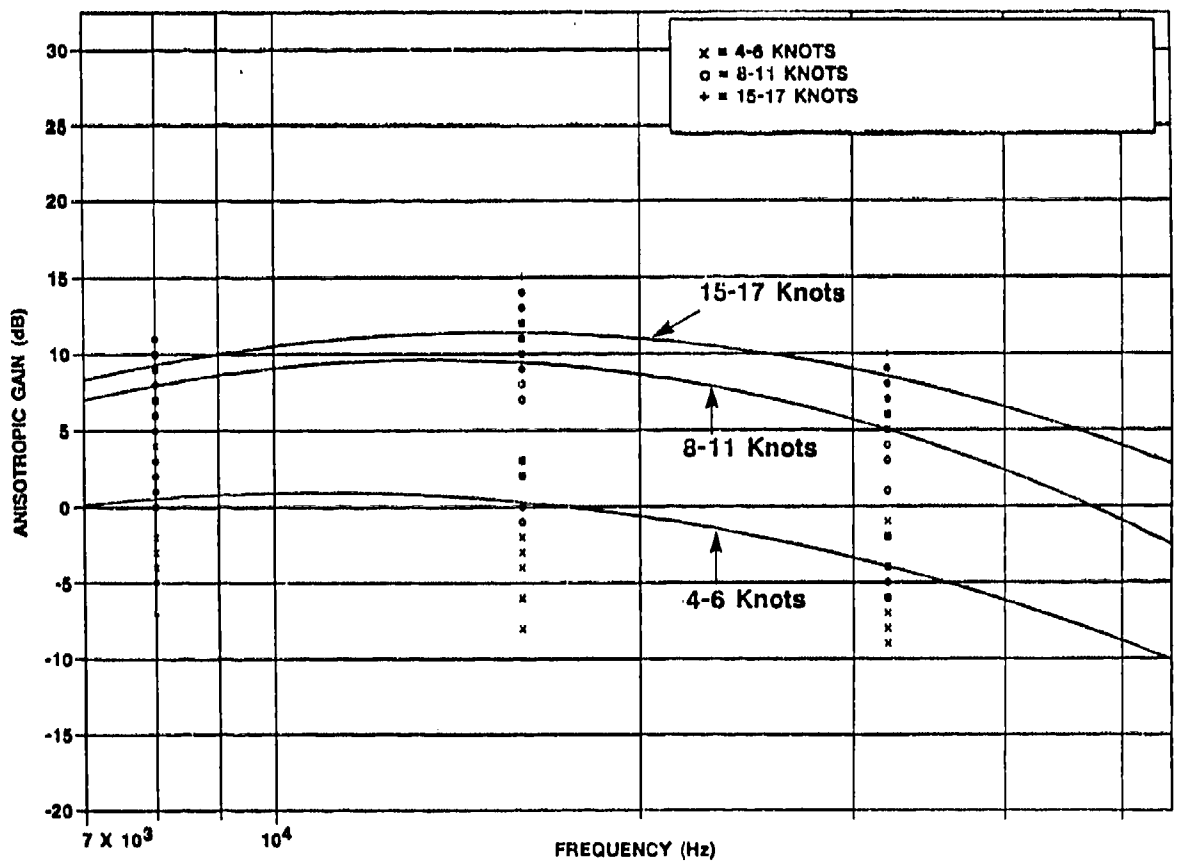

Figure 31. Frequency Dependence of Anisotropic Gain at Various Wind Speeds

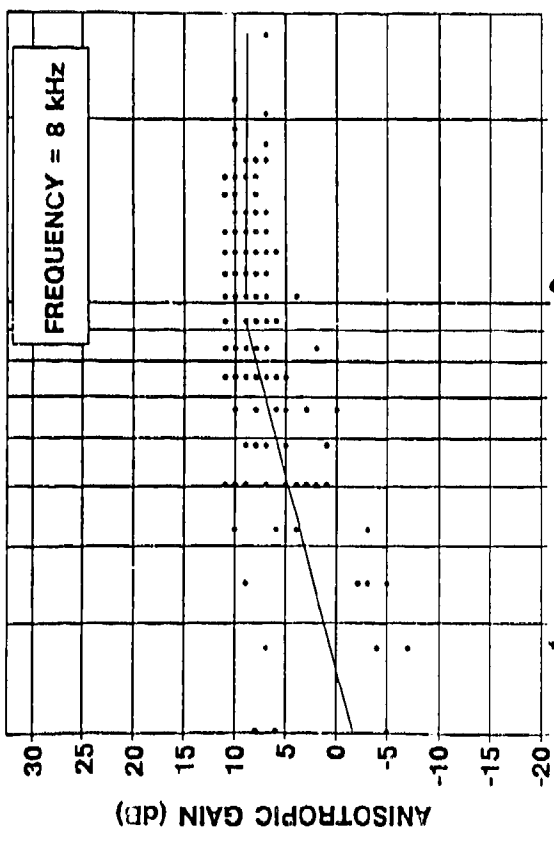

Figure 32. Anisotropic Gain Versus Nondimensional Friction Velocity at 8 kHz

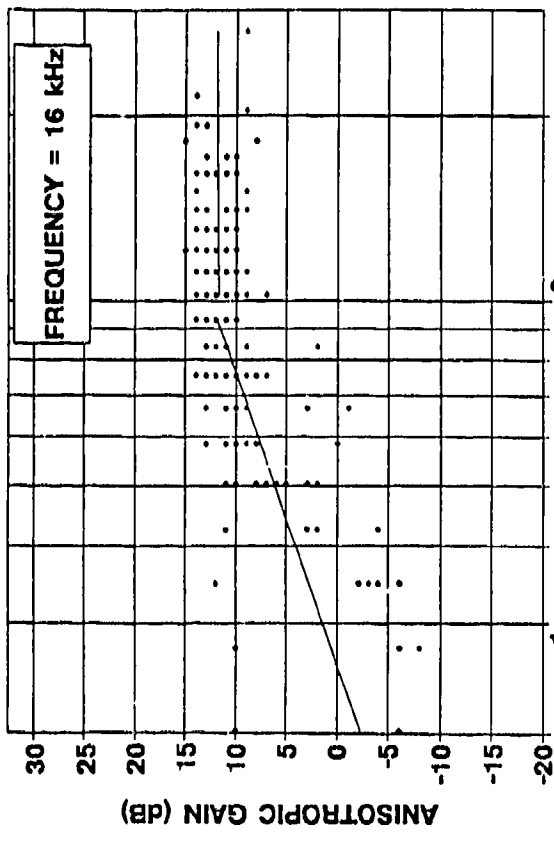

Figure 33. Anisotropic Gain Versus Nondimensional Friction Velocity at 16 kHz

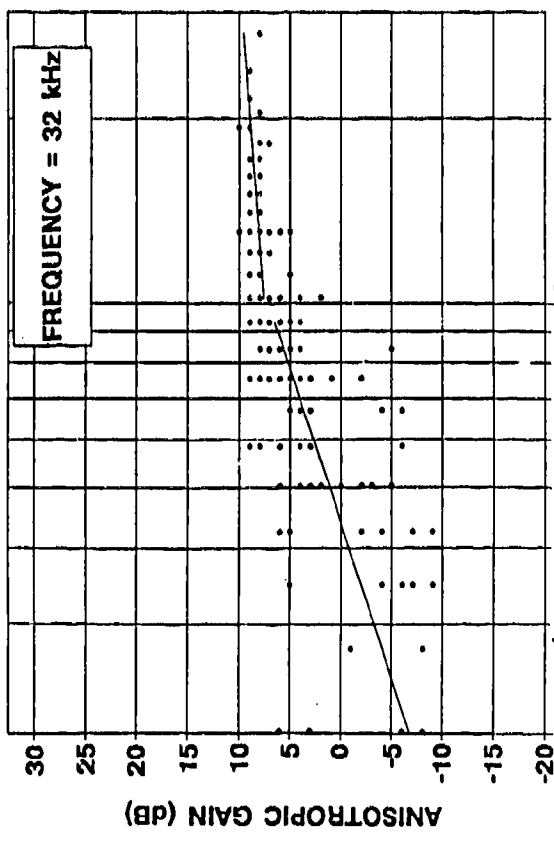

Figure 34. Anisotropic Gain Versus Nondimensional Friction Velocity at 32 kHz

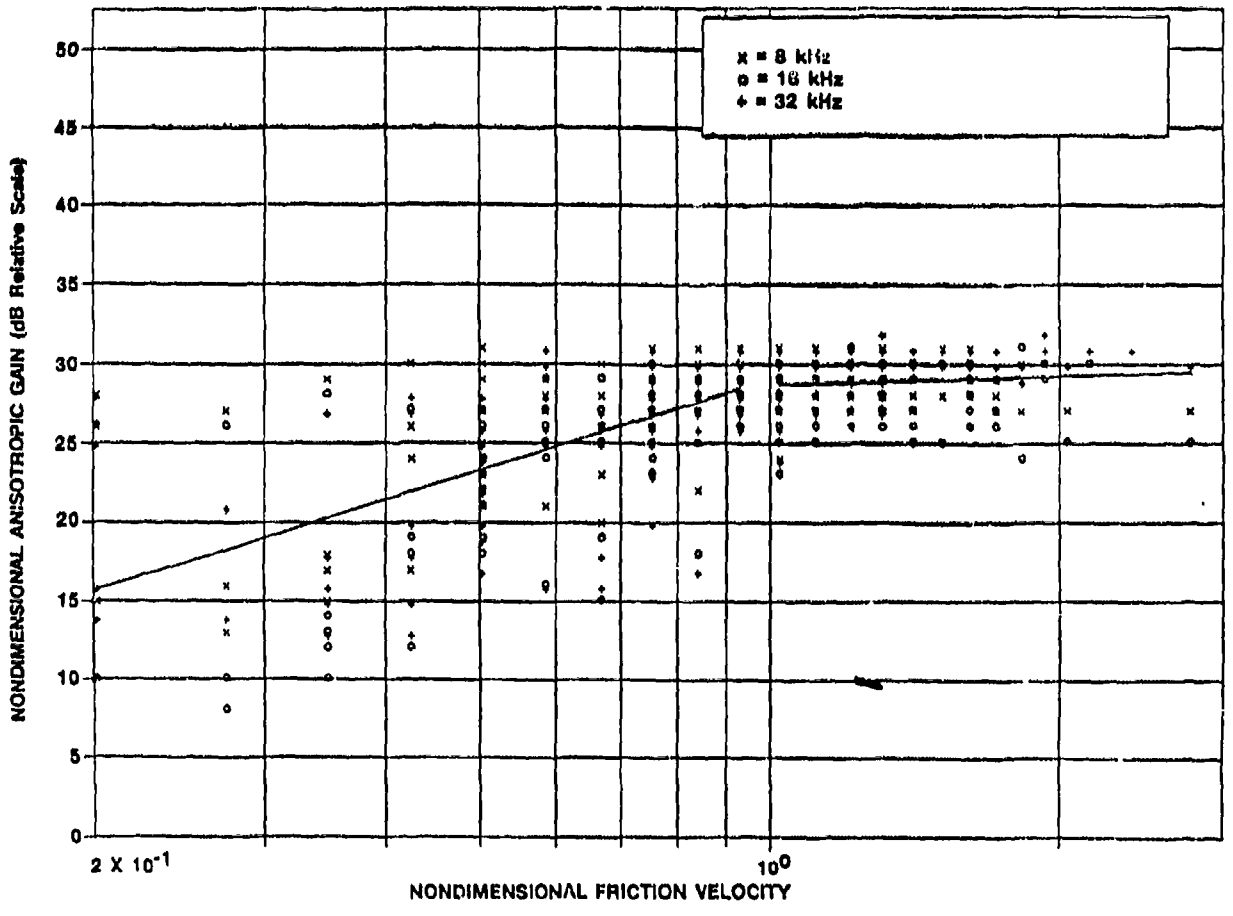

Figure 35. Composite Anisotropic Gain Versus Nondimensional Friction Velocity

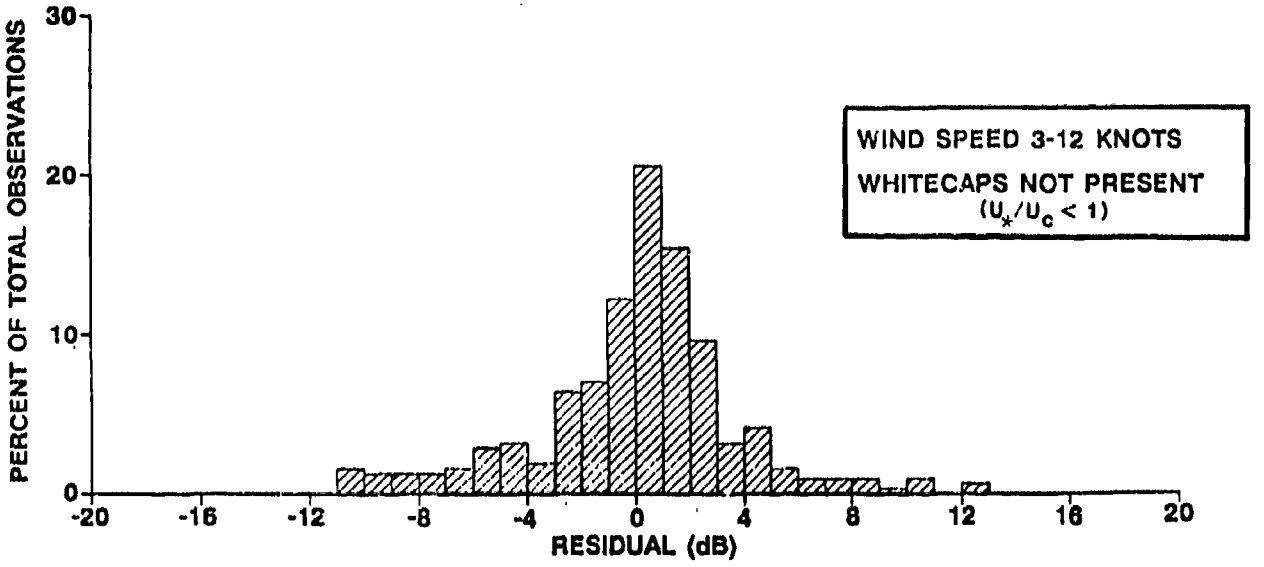

Figure 36. Histogram of Anisotropic Gain Residuals With Whitecaps Not Present

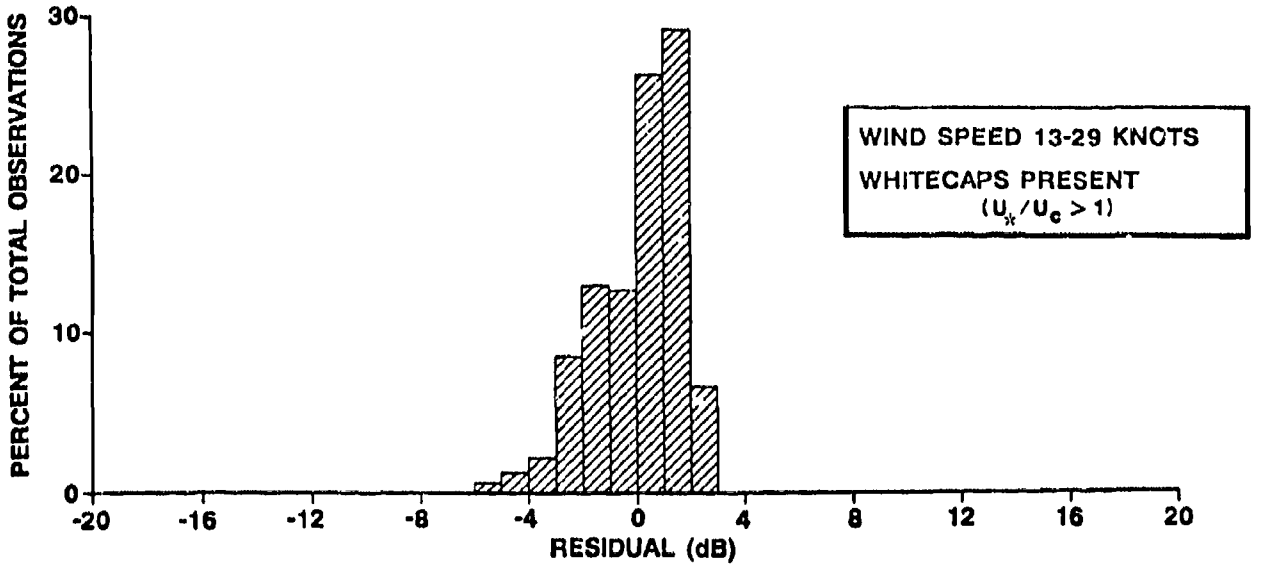

Figure 37. Histogram of Arisotropic Gain Residuals With Whitecaps Present

skewness.[29] This metric varied from 0.2 in the WNP case to 0.8 in the WP case. While no formal statement of statistical significance was worked out for this difference, it is clear that the WP case appears to have a physical upper limit and that all variation is constrained by this limit. This is not true in the WNP case which has symmetrical variation about the power law.

Let us return to the initial observation that the variability of the data in the WNP case is greater than in the WP case. One obvious possibility is that data contamination due to an electrical noise floor at the lower spectral levels of the WNP case is contributing to the variability. Another possibility is that without the uniform generation of spray and bubbles by the whitecaps, the sources of acoustic ambient are more irregular and dependent on an increased number of independent variables. Examples would be the distribution and excitation of bubbles due to the previous history of the sea conditions as well as the present state of the current, near-surface turbulence, and internal waves. An indication that the latter cause might be the case is illustrated in figures 38 to 40, which are plots of anistropic gain with total acoustic intensity as the independent variable. The idea is that the total acoustic intensity is a measure of the acoustic state of the sea, where, for a given wind speed (without whitecaps present), a range of acoustic states is possible and it is that range of conditions which caused the large variability being discussed. The reduced variability in the data at low acoustic intensity seen in the figures shows that total acoustic intensity is a better predictor of the anisotropic gain at low wind conditions than was wind speed-derived quantities. If the change in acoustic state were caused by sources which would be contaminants to the data, such as shipping or biological sources, then the resulting anisotropic gains would have been controlled by the sidelobes of the antenna, causing increases in the gain, and the variability would have increased rather than decreased, as was the case. In the next section we will argue that the range in acoustic states of the sea might be caused by the range in bubble layer depth. We note that some sound velocity-depth profile effects could be due to the refractive "hole" discussed in section 3. This would add variability to the anisotropic gain measurements both in the WP and WNP cases.

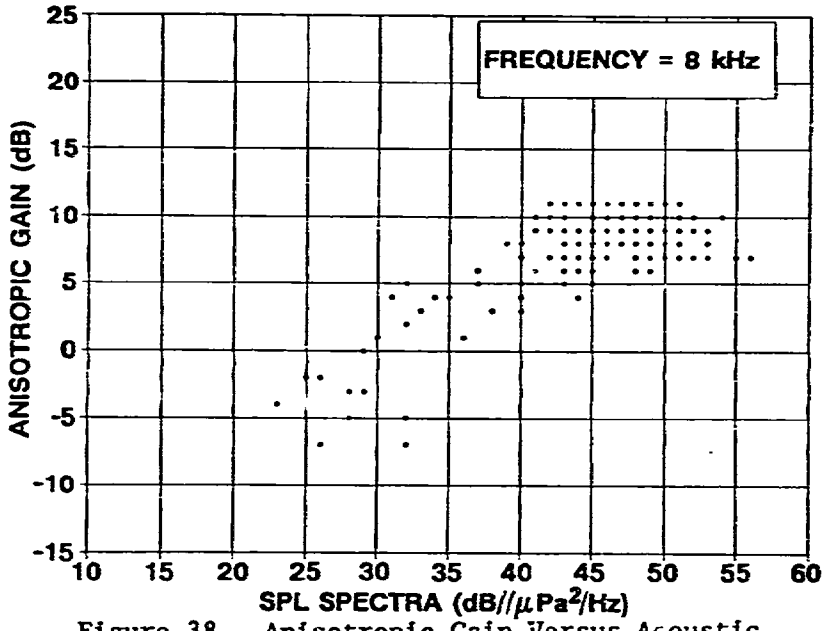

Figure 38. Anisotropic Gain Versus Acoustic SPL Spectra at 8 kHz

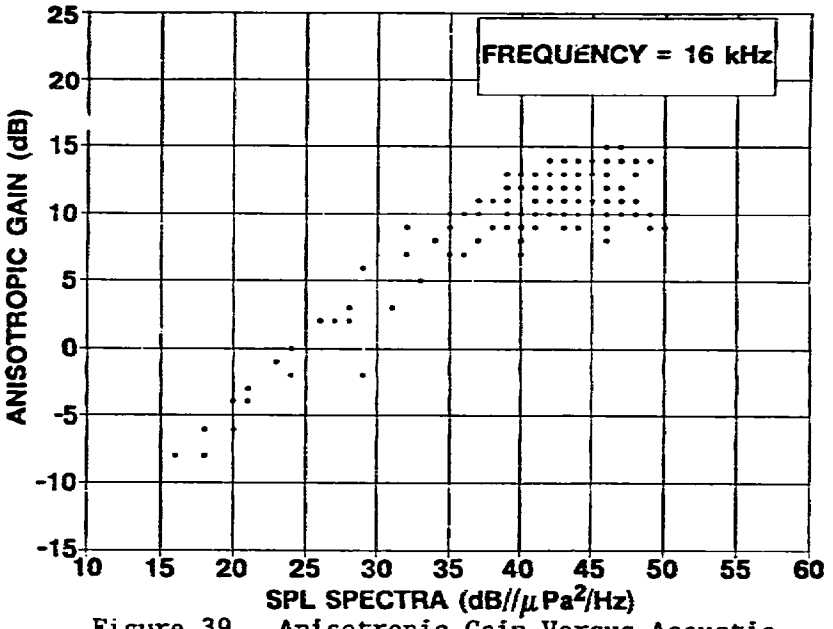

Figure 39. Anisotropic Gain Versus Acoustic SPL Spectra at 16 kHz

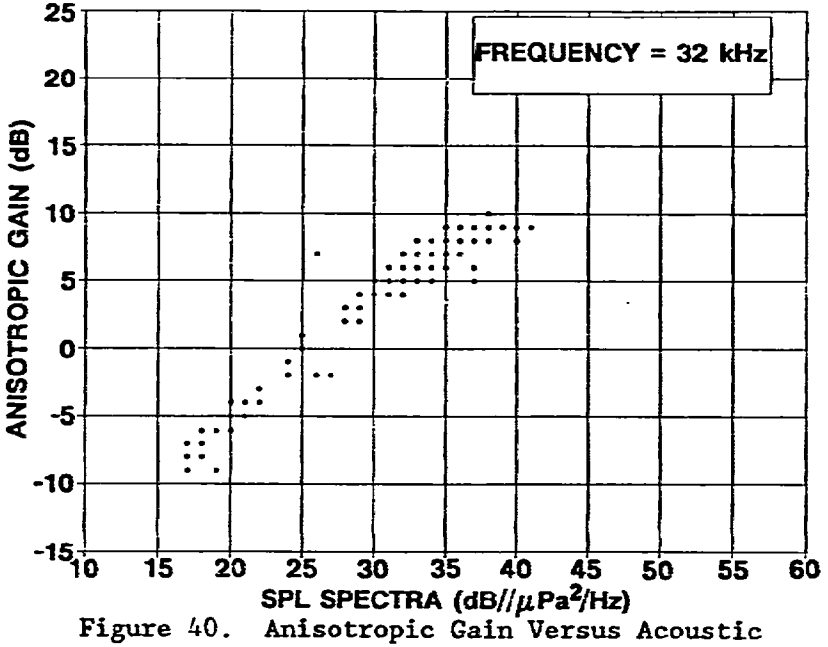

Figure 40. Anisotropic Gain Versus Acoustic SPL Spectra at 16 32 kHz

5.0 CONCLUSIONS

In this section we will draw some tentative conclusions about the cause of the high frequency acoustic ambient directivity spectra by bringing together the results of the theoretical discussions of section 2 and the measured results of section 4. The conclusions are necessarily tentative for two reasons: (1) the experiment only measured the horizontally directed acoustic ambient and is an incomplete observation, and (2) even complete knowledge of the sound field is not sufficient to determine uniquely the source as demonstrated by Dowling and Ffowcs Williams.[30]

We begin the discussion by reviewing the four basic observations of the experiment:

1. The anisotropic gain is a function of wind speed, as illustrated in figure 35.

2. The functional dependence of the anisotropic gain on wind speed is dichotomized according to whether or not whitecaps are present, as illustrated in figure 35.

3. The probability density function of the measured anisotropic gain at a given wind speed is skewed to lower values with whitecaps present, indicating a physical limit to the gain, as shown in figures 36 and 37.

4. The variability of the anisotropic gain without whitecaps present is significantly greater than with whitecaps present, and this variability is reduced by substituting total acoustic intensity for wind speed as the independent variable.

The derived quantity in the theoretical discussion of section 2 is the directivity spectra, while the measured quantity of section 4 is the line array beamformer output steered to the horizontal direction. The well-known relation between these two quantities, for an azimuthally uniform field, is

$$S_b^2(f) = 2\pi \int_0^{\pi} B(\phi,f)H_1(\phi,f)N(\phi,f) \sin\phi \, d\phi \qquad (33)$$

Thus, we can expect the horizontally directed beamformer output to be a sensitive measure of the vertical directional spectra in the horizontal direction. From section 2 we saw that the near-horizontal values of the directional spectra are the most physically revealing aspect of the function. This is true to the extent that the discussion is complete, i.e., the acoustic ambient diffuse sources consist of surface dipoles and below-surface monopoles only. These two source types lead to quite different source efficiencies at shallow "launch" angles. While the dipole is known to have a null in the horizontal direction, the layer of monopoles leads to a directional spectra that is determined by the integral of the vertical density distribution weighted by a factor that describes coherency of the surface reflection. This form is shown explicitly in equation (16). Thus a layer of monopoles beneath the ocean surface can asymptotically lead to either surface monopole-like or surface dipole-like behavior. The surface monopole-like behavior results from contributions of individual monopoles that are greater than a significant fraction of a wavelength from the sea surface, i.e., acoustically deep. As the depth of the individual contributors increases, the pattern function of the monopole source and its surface reflection produces a multipole function which, in concert with other such sources at incrementally different depths, leads to a composite monopole structure. Any reduction in the coherency of the surface reflection caused by a non-smooth function also produces a composite monopole structure. The surface dipole-like behavior results from the opposite conditions wherein all the subsurface monopoles are less than a small fraction of an acoustic wavelength from the surface (acoustically shallow), and the surface produces only specular reflections. Guo has pointed out that in this case the resulting dipole has a vanishingly small source level.[8] Changes in the behavior of the directional spectra of a below-surface layer of monopoles is best observed at near-horizontal angles, as illustrated in figures 3 through 5.

In the absence of surface dipole sources, the subsurface acoustically deep layer of monopole sources would lead to the situation in which the acoustic ambient is dominated by horizontally directed energy. This result would become more pronounced as the layer depth and/or surface roughness increases. Because the acoustically thin layer of monopoles leads to a vanishingly small dipole source, it is of little practical interest.[8,20] However, at the frequencies of interest in this report, surface dipole sources would result from sprays of droplets on the surface.[20,27] The surface dipole sources are known to lead to the situation in which the acoustic ambient is dominated by vertically directed energy. Thus, when evaluating the anisotropic gain for horizontal steering, the surface monopole and surface dipole cases lead to distinctly different values. In the former case one is "looking away from the noise," i.e., high array gain, and in the latter case one is "looking into the noise," i.e., low array gain. Furthermore, we note that the surface dipole case leads to a maximum gain situation; i.e., the maximum possible gain in the horizontal direction occurs when the acoustic ambient is caused by a surface layer of dipole sources.

The above models can be shown to fit qualitatively our experimental observations as follows:

1. A wind speed-dependent array gain would be expected if the wind and the resulting sea changed the source structure from surface dipoles to a subsurface layer of acoustically deep monopoles, presumably oscillating bubbles. Furthermore, the wind, as well as other factors, would be expected to change the vertical distribution of the monopole density, and such changes would change the array gain.

2. With whitecaps present the acoustic sources would be expected to be dipole-like as a result of a ready supply of spray and acoustically thin layers of bubbles. These dipoles would minimize the horizontal values of the ambient directional spectra so that the horizontally steered array gain would exceed the directivity function. In fact there would be a maximum value determined by a pure surface dipole source. Thus the largest values of the horizontally steered array gain would be expected to occur with whitecaps

present, as the measurements indicated. Furthermore, because an array gain maximum exists, the statistical distribution of values would be skewed to lower values, as was measured.

3. With no whitecaps present the supply of spray and acoustically thin layers of monopoles would be significantly diminished. In the absence of these sources the role of an acoustically thick layer of bubbles would become more important. The presence of this layer of sources would increase the horizontal values of the directivity function relative to the vertical values and the array gain would be expected to be lower than was the case when whitecaps were present, as occurred in the data. Because the wind would not be the only cause for the vertical distribution of the monopoles, one would expect a significant range of conditions to exist at a particular wind speed. This variability was certainly present in the experiment results.

4. If the above reasoning is correct, then the data argue that in general the vertical depth scale of the monopole layer increases with decreasing wind speed although with significant variation in the value for a given wind speed. The depth scale variation, or more exactly the array gain variation, is directly related to the total acoustic intensity of the acoustic ambient, which serves as a good predictor of the directional spectra.

6.0 REFERENCES

1. W.A. Von Winkle and D.G. Browning, Vertical Noise Directionality in the Deep Ocean: A Review, NUSC Technical Document 7561 , Naval Underwater Systems Center, New London, CT, 1985 (UNCLASSIFIED).

2. R.J. Urick, Ambient Noise in the Sea, Peninsula Publishing, 1984.

3. R.M. Hamson, "The Theoretical Responses of Vertical and Horizontal Line Arrays to Wind Induced Noise in Shallow Water," Journal of the Acoustical Society of America, vol. 78, 1985, pp 1702-1712.

4. W.A. Kuperman and F. Ingenito, "Spatial Correlation of Surface Generated Noise in a Stratified Ocean," Journal of the Acoustical Society of America, vol. 67, 1980, pp 1988-1996.

5. N. Yen and A.J. Perrone, NUSC Technical Report 5833, "Mechanisms and Modeling of Wind Induced Low Frequency Ambient Sea Noise," Naval Underwater Systems Center, New London, CT, 1979 (UNCLASSIFIED).

6. H. Li, "On Wind Induced Underwater Ambient Noise," NORDA Technical Note 89, Naval Ocean Research and Development Agency, Bay Saint Louis, MS., 1981 (UNCLASSIFIED).

7. B.R. Kerman, "Underwater Sound Generation by Breaking Waves," Journal of the Acoustical Society of America, vol. 75, 1984, p 148.

8. Y.P. Guo, "Sound Generation in the Ocean by Breaking Surface Waves," Journal of Fluid Mechanics, vol. 181, 1987, pp 329-347.

9. A. Prosperetti and N.Q. Lu, "Cavitation and Bubble Bursting as Sources of Oceanic Ambient Noise," Journal of the Acoustical Society of America, vol. 84, 1988, pp 1037-1041.

10. L.M. Lyamshev, A.V. Furduev, and B.I. Chelnokov, "A Mechanism of Generation of Underwater Acoustic Noise in the Ocean During a Calm," Soviet Physics-Acoustics, vol. 31, 1985, pp 435-436.

11. W.S. Liggett and M.J. Jacobsen, "Covariance of Surface Generated Noise in a Deep Ocean," Journal of the Acoustical Society of America, vol. 38, 1965, pp 303-312.

12. B.F. Cron and C.H. Sherman, "Spatial Correlation Functions for Various Noise Models," Journal of the Acoustical Society of America, vol. 34, 1962, pp 1732-1736.

13. E.H. Axelrod, B.A. Schoomer, and W.A. Von Winkle, "Vertical Directionality of Ambient Noise in the Deep Ocean at a Site Near Bermuda," Journal of the Acoustical Society of America, vol. 37, 1965, pp 77-83.

14. A.S. Burgess and D.J. Kewley, "Wind Generated Surface Noise Source Levels in Deep Water East of Australia," Journal of the Acoustical Society of America, vol. 73, 1983, pp 201-210.

15. R.J. Urick, Principles of Underwater Sound, 2nd ed., McGraw-Hill Book Company, New York, NY, 1975.

16. C.S. Clay and H. Medwin, Acoustical Oceanography, Principles and Applications, John Wiley & Sons, New York, NY, 1977.

17. S.O. McConnell, "Acoustic Measurements of Bubble Densities at 15-50 kHz," Sea Surface Sound, edited by B.R.Kerman, Kluwer Academic Publishers, Boston, MA, 1988.

18. G.B. Crawford and D.M. Farmer, "On the Spatial Distribution of Ocean Bubbles," Journal of Geophysical Research, vol. 92, no. c8, July 1987, pp 8231-8243.

19. R.W. Bannister, A.S. Burgess, and D.J. Kewley, "Estimation of Source Characteristics From Underwater Noisefield Measurements, Sea Surface Sound, edited by B.R. Kerman, Kluwer Academic Publishers, Boston, MA, 1988.

20. J.E. Ffowcs Williams and Y.P. Guo, "Mechanisms of Sound Generation at the Ocean Surface," Sea Surface Sound, edited by B.R. Kerman, Kluwer Academic Publishers, Boston, MA, 1988.

21. R.D. Hallett and R.M Heitmeyer, "Noise Generation by Bubbles Formed in Breaking Waves," Sea Surface Sound, edited by B.R. Kerman, Kluwer Academic Publishers, Boston, MA, 1988.

22. R.M. Kennedy and T.K. Szlyk, "A Multipath Calculation of Underwater Acoustic Vertical Directivity in the Tongue of the Ocean," NUSC Technical Memorandum 883007, Naval Underwater Systems Center, New London, CT, August 1988 (UNCLASSIFIED).

23. H.W. Marsh and M. Schulkin, "Report on the Status of Project AMOS," NUSL Report 255A, Naval Underwater Sound Laboratory, New London, CT, 1955, revised May 1967.

24. H. Cox, "Spatial Correlation in Arbitrary Noise Fields With Application to Ambient Sea Noise," Journal of the Acoustical Society of America, vol. 54, no. 5, 1973, pp 1289-1301.

25. J. Wu, "Wind-Stress Coefficients Over Sea Surface Near Neutral Conditions - a Revisit," Journal of Physical Oceanography, vol. 10, 1980, pp 727-740.

26. A.B. Caron and E.S. Sheffield, "AUTEC Ambient Noise Analysis, Descriptions of Data and Analyses," NUSC Informal Memorandum, Naval Underwater Systems Center, New London, CT, 13 July 1988.

27. D. Ross, Mechanics of Underwater Noise, Pergamon Press, Elmsford, NY, 1976.

28. A. Prosperetti, "Bubble Related Ambient Noise in the Ocean," Journal of the Acoustical Society of America, vol. 84, no. 3, September 1988.

29. G.A. Korn and T.M. Korn, Mathematical Handbook for Scientists and Engineers, McGraw-Hill Book Company, New York, NY, 1968.

30. A.P. Dowling and J.E. Ffowcs Williams, Sound and Sources of Sound, John Wiley & Sons, New York, NY, 1983.

INITIAL DISTRIBUTION LIST

Addressee	Number of Copies
COMNAVSEASYSCOM (Code 63D) CDR E. Graham	1
(PMS393A) CDR S. Logue	1
(PMS393N) J.H. Fuchs	1
COMNAVAIRSYSCOM (Code 421) T. Ramirez	1
CNA	1
DTIC	12
DTRC (Code 1925) G.M. Jebsen	1
(Code 0100) R.E. Metrey	1
NAVPGSCOL H. Medwin	2
NOAA/Miami H. Bezdek	1
NOSC J. Rohn	1
OCNR (Code 1121GS) O. Brandt	1
(Code 1122ML) M. Briscoe	1
(Code 1125) L.G. Johnson	1
(Code 1125AR) R.F. Obrachta	1
(Code 11250A) M. Orr	1
Applied Measurement Systems, Inc., Hollywood, FL; B.L. Douglass	1
General Electric Co., Andros Island, Bahamas; L.A. Lindquist	1
GRD Associates, Delray Beach, FL; G.R. Desmarais	1
Planning Systems, Inc., New London, CT; W.M. Leen	1
MPL, Scripps Institution of Oceanography, La Jolla, CA; W. Hodgekist	1